

Figure 3-19. Histogram of isotopic ratios for 741 Study Area probes.

Table 3-9. Comparison of expected and observed Pu, Am, and Np activity ratios.

Ratio	Weapons-Grade Pu	Observed
$^{239}\text{Pu}:$ $^{241}\text{Am}$	6.7	<1
$^{241}\text{Am}:$ $^{237}\text{Np}$	100,000	30,000

Table 3-10. 741 Study Area probe holes selected for azimuthal logging.

Probe Hole	Depth (ft)	Radionuclide	Maximum cps <sup>a</sup>
741-08	8.0	$^{237}\text{Np}^b$	316
741-02	11.5	$^{237}\text{Np}^b$	428
741-04	9.5	$^{237}\text{Np}^b$	172
741-03	9.5	$^{237}\text{Np}^b$	244

a. As observed by standard gamma-ray logging.

b.  $^{237}\text{Np}$  indicated by  $^{233}\text{Pa}$  daughter.

Azimuthal logging was conducted by GTS Duratek during May 2001, and preliminary results were delivered to the INEEL on May 31, 2001. Azimuthal logs were analyzed to choose probes for follow-up studies of  $^{237}\text{Np}$  leaching and migration. Azimuthal data were used to indicate the position of  $^{237}\text{Np}$  relative to the probe hole so that lysimeters could be installed to collect leachate samples.

For each probe, Table 3-11 lists detected radionuclides and gives the azimuth of the observed maximum count rate for each. Azimuth is measured with respect to a north arrow marked on the probe casing. Table 3-11 also gives the approximate maximum count rates and two general qualifiers. The first qualifier describes the statistical significance of the direction indication, and the second qualifier describes the narrowness of the direction indication (i.e. "good" indicates a highly directional source, and "poor" indicates a broadly directional source).

The Table 3-11 data were used to determine the position and target depth for Type B probes. These data may also be used to choose locations for additional Type A probes in the event that it becomes necessary to model the radionuclide source distribution in detail.

### 3.2.4 Cluster Probe Analysis

Offset probes to Probe Hole 741-08 were installed to the WSW, approximately 150 degrees to the high  $^{239}\text{Pu}$  direction as indicated by azimuthal logging (Figure 3-20). Logging data from the offset probes showed no indication that the  $^{239}\text{Pu}$  source extends toward the WSW. The three probe pattern at this location is not a good candidate for further study of the  $^{239}\text{Pu}$  source.

Table 3-11. 741 Study Area azimuthal data summary.

Probe	Depth (ft)	Nuclide @ Azimuth	Maximum m cps	Statistics	Direction
741-08	8.0	233Pa @ 125 degrees	2.5	Fair	Good
		241Am @ 115 degrees	3.5	Fair	Fair
		239Pu @ NA	2.8	Good	Poor
741-02	11.5	233Pa @ 85 degrees	5.5	Good	Fair
		241Am @ 80 degrees	6.2	Good	Fair
		239Pu @ 85 degrees	0.6	Poor	Good
		583 keV @ 80 degrees	0.8	Fair	Fair
741-04	9.5	233Pa @ 200 degrees	1.4	Good	Poor
		241Am @ 205 degrees	2.0	Good	Poor
		239Pu @ 180 degrees	0.4	Poor	Good
741-03	9.5	233Pa @ 35 degrees	2.4	Good	Fair
		241Am @ 35 degrees	3.3	Good	Fair

### 3.3 Depleted Uranium Focus Area

The primary objective of the DU Study Area investigation is to assess the solubility of uranium and its potential for transport in groundwater. Uranium solubility is highly dependent on the uranium valence state (i.e., the chemical form). Nuclear logging cannot directly distinguish uranium chemical forms but may be used in combination with leachate samples to develop groundwater release models. Groundwater release models compare the amount and distribution of uranium, the soil moisture conditions, and the concentration of dissolved uranium in leachate to determine solubility and release parameters. These models provide an estimate of uranium solubility and release potential (see Figure 3-16).

Inventory records indicate that, in terms of mass percentage, DU constitutes the majority of the disposed uranium at the SDA. Because it is the predominant uranium waste form, DU waste was sought as the target for the groundwater release studies. Downhole logging data may provide a basis to differentiate DU waste from other uranium waste. Downhole logging data also provide the best means to estimate the amount and distribution of DU as required for the release models.

#### 3.3.1 Selection of Probe Locations

Figure 3-21 shows inventory information used for selecting probe locations in the DU Focus Area. The inventory data showed a concentration of RFP drums containing uranium waste in the far western portion of Pit 10. Geophysical data were interpreted to indicate the location of concentrated metallic debris, such as 55-gal drums. Accordingly, the initial DU Focus Area exploratory probes (DU-01–DU-08) were arranged as two profiles and positioned to intersect geophysical anomalies within the uranium drum area. Nine additional probes (DU-09–DU-17) were later added to expand the subsurface investigation area and follow trends observed in the original probes. Figure 3-22 shows the surface geophysics data and the final location of the DU Focus Area probes.

# 741-08 OFFSET PROBES SUMMARY

Pu AZIMUTHAL LOG @ 8.0 FT  
 SELECTED STANDARD LOGS

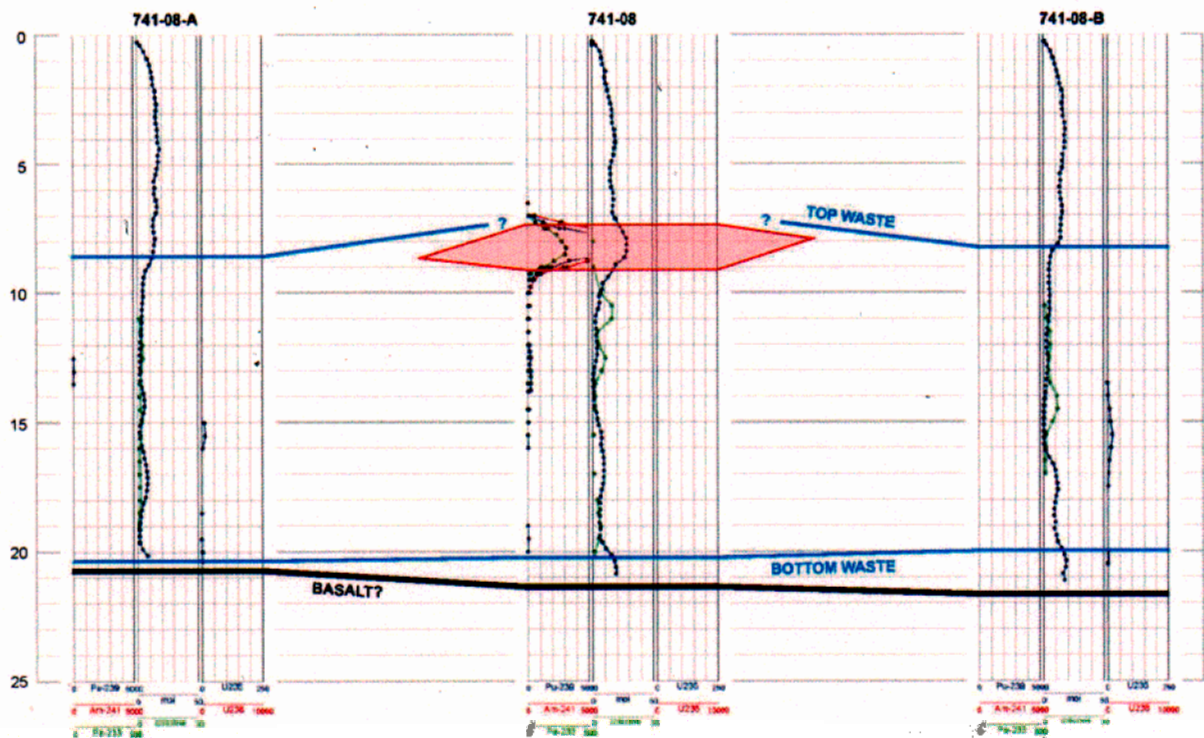
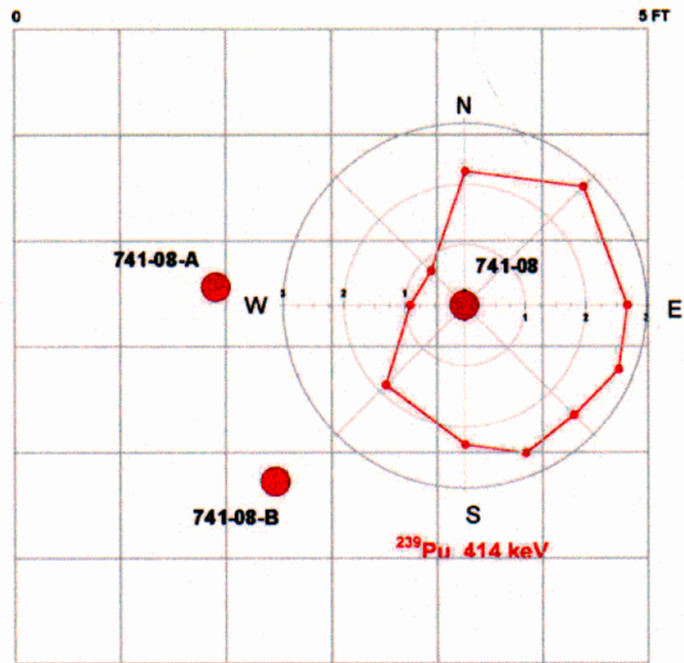


Figure 3-20. Cross section through partial probe cluster at Probe Hole 741-08. ...

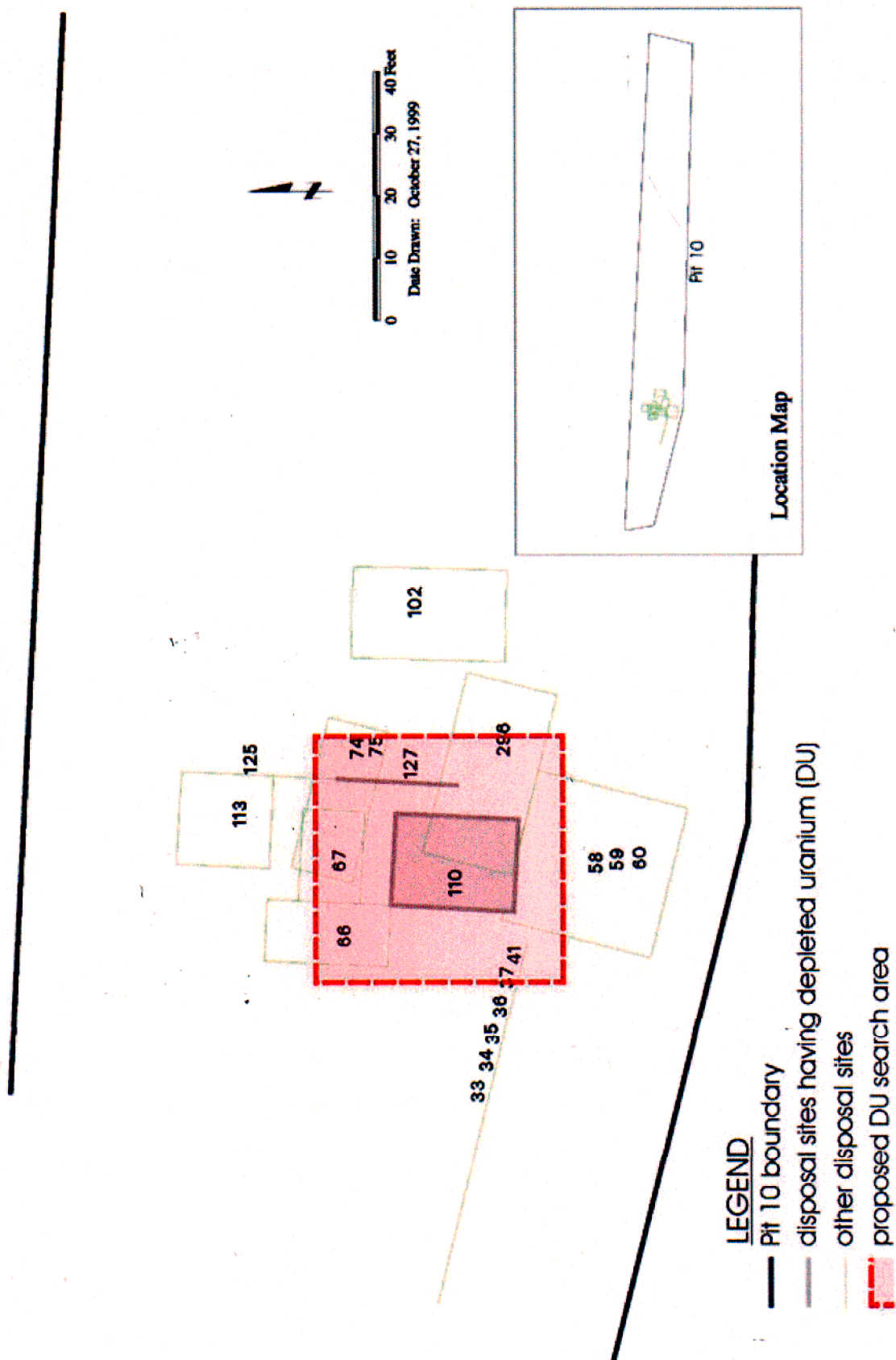


Figure 3-21. Inventory records for the Depleted Uranium Focus Area.

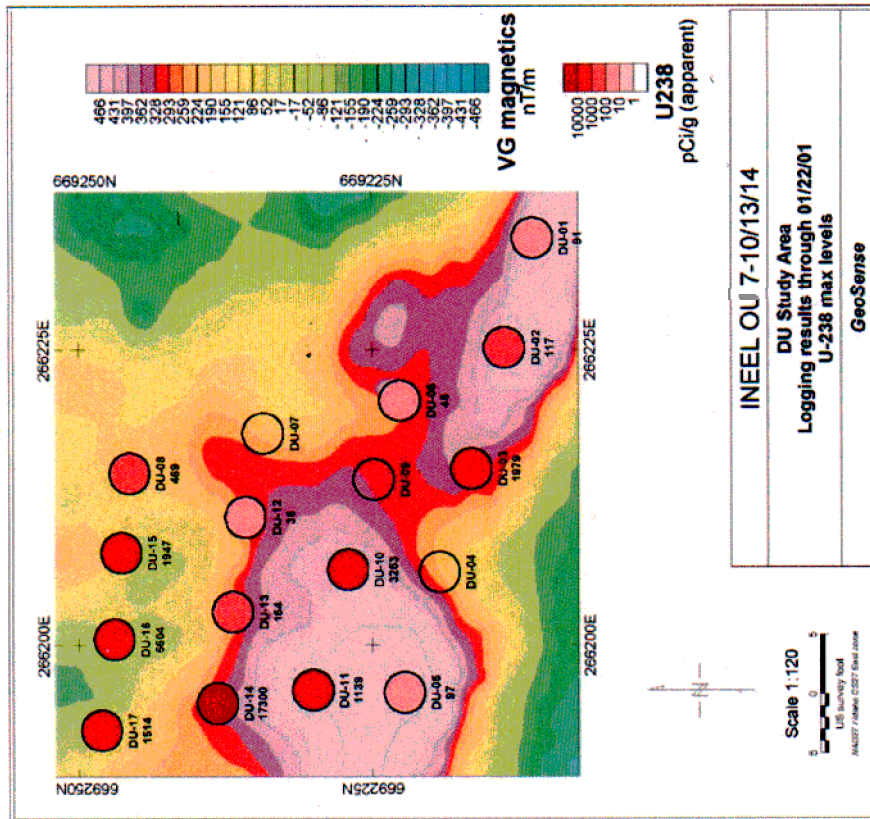
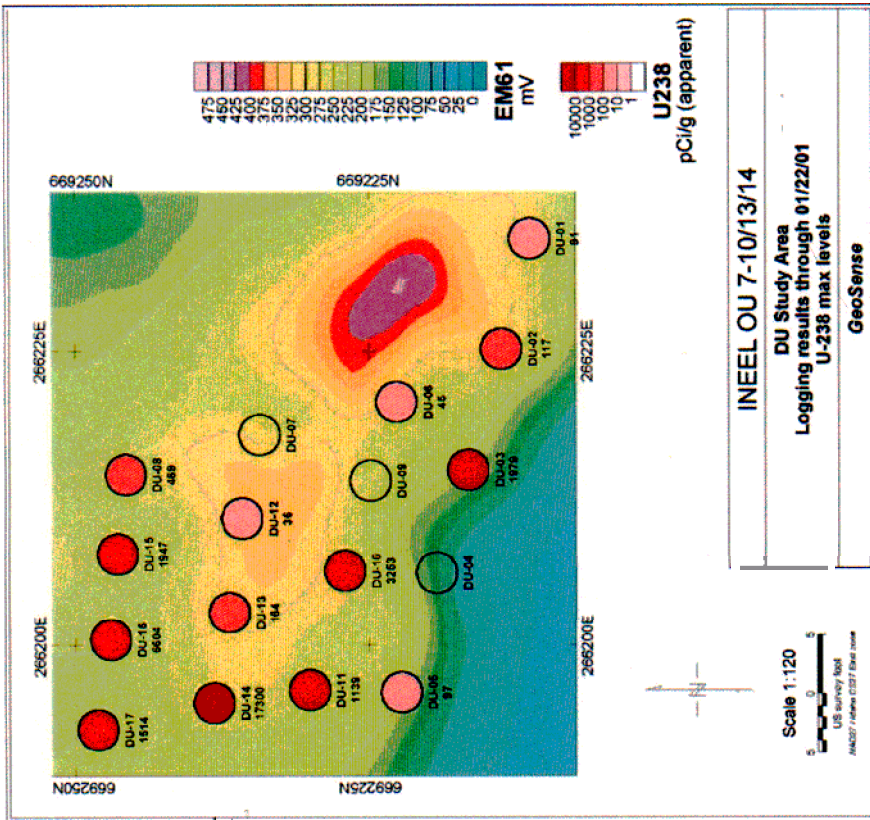


Figure 3-22. Surface geophysics for the Depleted Uranium Focus Area. Final probe locations are also shown.

### 3.3.2 Observations on Radionuclide Contamination

The logging subcontractor conducted preliminary processing of the DU and 741 Study Area logging data. Their processing included automated spectral analysis of passive gamma-ray data to identify the presence of specific target contaminants including  $^{235}\text{U}$ ,  $^{238}\text{U}$ ,  $^{239}\text{Pu}$ ,  $^{241}\text{Am}$ , and  $^{237}\text{Np}$ . After applying a standard calibration correction to convert net count rates to apparent radionuclide concentrations, summary results were compiled and delivered to the INEEL along with the raw spectral data.

Table 3-12 below gives maximum detected levels of key target contaminants for all DU Area probes. Blank cells indicate nondetects.

The initial eight DU probes ranged in depth from 12 to 18 ft and showed a single uranium and chlorine contamination zone in the 5–10-ft depth range, except at one end, which has an upper chlorine contamination zone overlaying a lower chlorine, uranium, and plutonium contamination zone (Figure 3-23).

Pu, Am, and Np are observed in various combinations throughout the DU Study Area with higher relative amounts of Pu compared to other areas of Pits 4, 9, and 10. Probe DU-15 shows an apparent  $^{239}\text{Pu}$  concentration just under 50,000 nCi/g or about 25% of the level observed in P9-20.

Table 3-12. Radionuclide detection summary for Depleted Uranium Focus Area.

Well ID	Cl_1,165 cps	Cl_6,111 cps	$^{235}\text{U}$ _186 pCi/g	$^{238}\text{U}$ _1,001 pCi/g	$^{239}\text{Pu}$ _414 nCi/g	$^{241}\text{Am}$ _662 nCi/g	$^{233}\text{Pa}$ _312 pCi/g
DU-01	23	10	1	91	ND	ND	ND
DU-02	5	3	6	117	33	179	5
DU-03	20	8	14	1,979	ND	ND	ND
DU-04	ND	ND	ND	ND	ND	128	ND
DU-05	2	1	ND	97	ND	ND	ND
DU-06	22	10	ND	45	ND	ND	0
DU-07	4	3	ND	ND	64	41	ND
DU-08	21	9	18	469	4,944	ND	4,881
DU-09	21	8	ND	ND	ND	ND	ND
DU-10	10	4	ND	3,253	ND	ND	ND
DU-11	11	4	11	1,139	776	58	1
DU-12	NL	NL	2	36	12	ND	2
DU-13	NL	NL	73	164	804	63	4
DU-14	NL	NL	ND	17,300	339	33	ND
DU-15	NL	NL	17	1,947	48,699	4,878	164
DU-16	NL	NL	9	6,604	ND	ND	ND
DU-17	NL	NL	2	1514	446	46	4

ND = nondetect  
NL = not logged

# DEPLETED URANIUM STUDY AREA

Cross sections showing:

- MOISTURE
- PASSIVE NEUTRON
- N-GAMMA CHLORINE\*
- SPECTRAL GAMMA U238\*
- SPECTRAL GAMMA U235\*

\*ESTIMATED CONCENTRATIONS ASSUME HOMOGENEOUS, ISOTROPIC, UNCONSOLIDATED SOIL

## KEY

- U238, U235 ZONES
- CL ZONES
- REFUSAL DEPTH

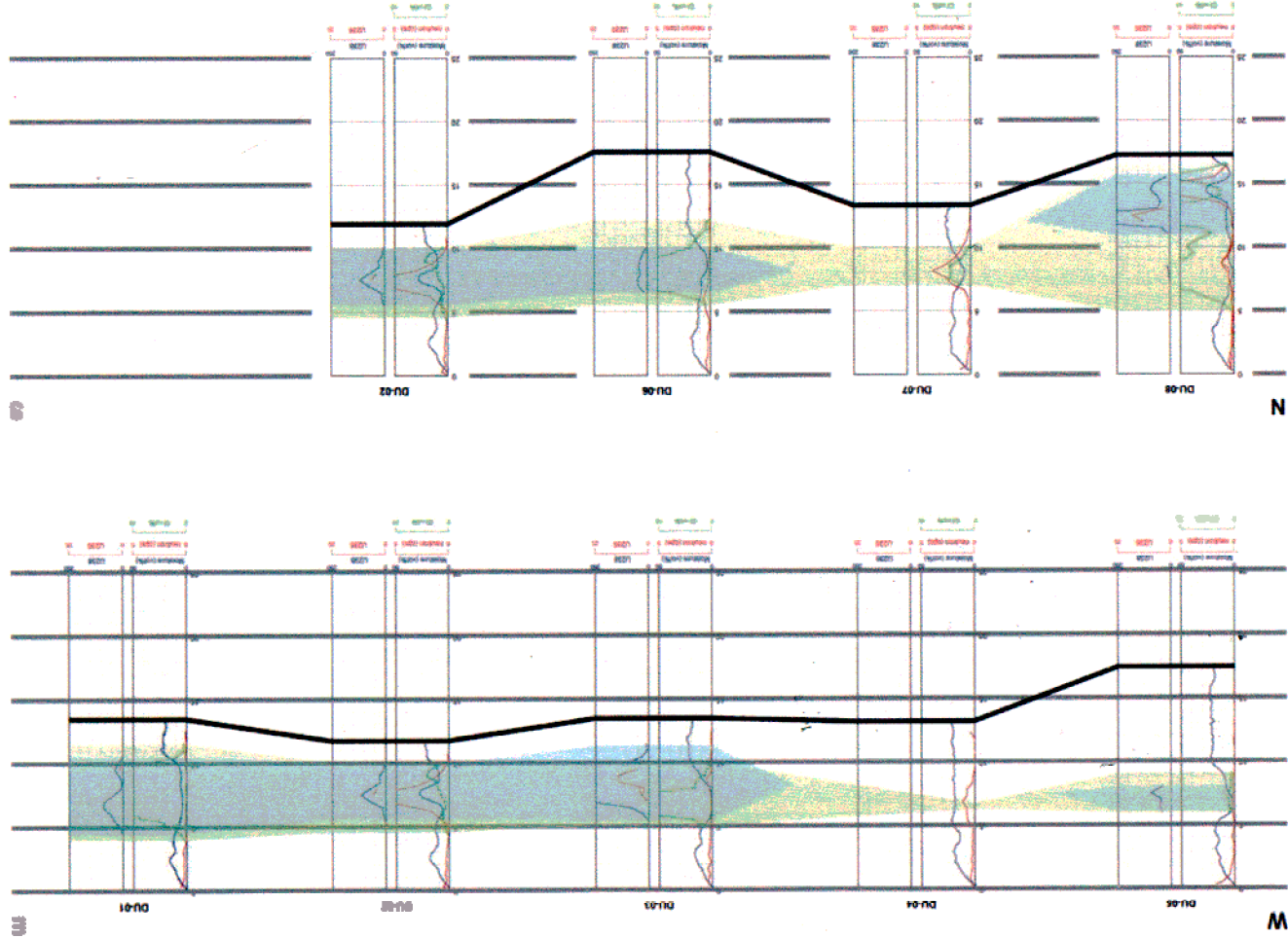
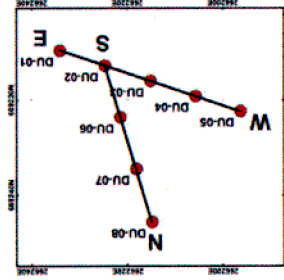


Figure 3-23. Cross section summary for Depleted Uranium Study Area.

The following observations relate to the nine additional DU probes:

- Levels of  $^{238}\text{U}$  were more widespread in the new probes than in the original eight probes. Three of the new probes had higher apparent  $^{238}\text{U}$  concentrations than previously observed in the DU Study Area. DU-14 had an apparent  $^{238}\text{U}$  concentration of 17,300 pCi/g (compared to a previous high in DU-03 of 1,979 pCi/g).
- Levels of  $^{235}\text{U}$  observed in the new probes are comparable to those observed in the original 8 probes. DU-13 had an apparent  $^{235}\text{U}$  concentration of 73 pCi/g (compared to a previous high in DU-08 of 18 pCi/g). As before,  $^{235}\text{U}$  is often not detected above the noise level even when  $^{238}\text{U}$  is prominent. Locations for Probes DU-09–DU-17 were chosen partly on the basis of surface geophysical data to give a comparison between probes positioned at the peaks of geophysical anomalies (i.e. where magnetic and electromagnetic data indicated higher metallic waste content) and probes located on the flanks of geophysical anomalies (i.e., where magnetic and electromagnetic data indicated lesser metallic waste content). The logging data show that radionuclides were detected in all locations and that variations in apparent radionuclide concentration are unrelated to the metallic waste content as indicated by the geophysical data (see Figure 3-22).

Two DU Study Area probe holes were selected for further study. The primary recommended cluster probe target in the DU Study Area occurs in Probe Hole DU-03 at a depth of 9 ft. This zone has the following attributes:

- Both  $^{238}\text{U}$  and  $^{235}\text{U}$  were observed in high concentrations compared with other DU Area probe holes
- Both  $^{235}\text{U}$  and  $^{238}\text{U}$  ratios are consistent with depleted uranium
- No other intermixed contamination observed
- Reduced contamination level for several feet below high contamination zone provides convenient conditions for leachate collection and migration studies.

The secondary recommended cluster probe target in the DU Study Area occurs in Probe Hole DU-08 at a depth of 12.5 ft. This zone has the following attributes:

- Both  $^{238}\text{U}$  and  $^{235}\text{U}$  were observed in high concentrations compared with other DU Area probe holes
- Both  $^{235}\text{U}$  and  $^{238}\text{U}$  ratios are consistent with natural uranium
- Pu, Am, and Np occur within same depth zone as  $^{235}\text{U}$  and  $^{238}\text{U}$
- Both  $^{235}\text{U}$  and  $^{238}\text{U}$  occur near bottom of the hole.

**3.3.2.1 Plutonium, Americium, and Neptunium.** Pu:Am and Am:Np apparent activity ratios for DU Area probes are shown in Figure 3-24. Computed ratios assume homogenous conditions and do not account for differential attenuation of gamma rays.

Table 3-13 shows a comparison between expected and observed Pu, Am, and Np ratios where the expected values are based on 30-year decay of weapons-grade plutonium. The Am:Np ratio suggests an excess of Np relative to the amount expected from pure Am decay.

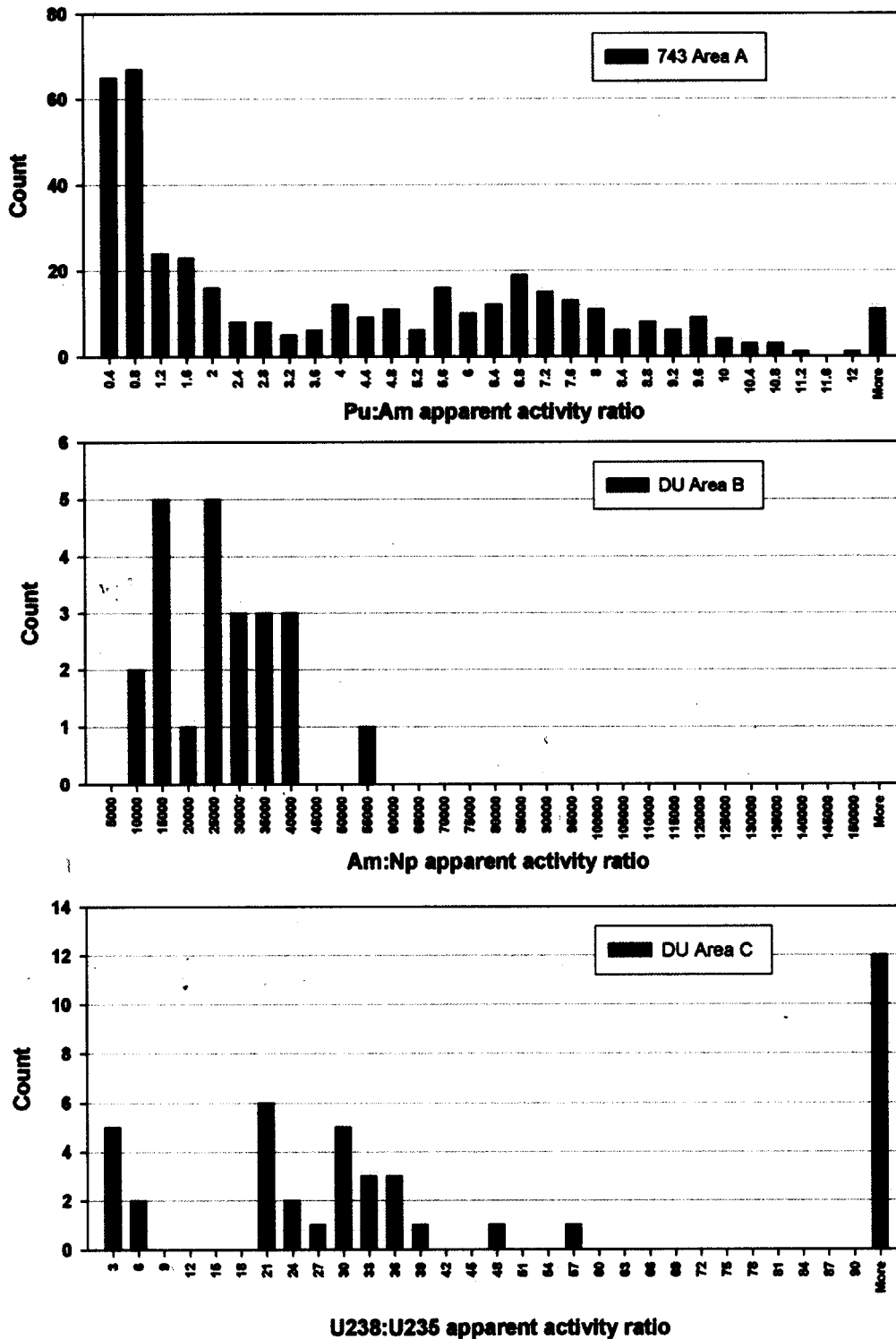


Figure 3-24. Histogram of isotopic ratios for Depleted Uranium Study Area probes.

Table 3-13. Comparison of expected and observed Pu, Am, and Np activity ratios.

Ratio	Weapons-Grade Plutonium	Observed
$^{239}\text{Pu}:^{241}\text{Am}$	6.7	6–8
$^{241}\text{Am}:^{237}\text{Np}$	100,000	10,000–40,000

**3.3.2.2 Uranium-235 and Uranium-238.** Figure 3-24 shows  $^{238}\text{U}:^{235}\text{U}$  apparent activity ratios for DU Study Area probes. Computed ratios assume homogenous conditions and do not account for differential attenuation of gamma rays.

Concentration ratios  $^{238}\text{U}:^{235}\text{U}$ , uncorrected for differential attenuation, show two trends:  $^{238}\text{U}:^{235}\text{U} > 100$  and  $^{238}\text{U}:^{235}\text{U} = 21 - 36$ . Uranium isotopic ratios are most consistent with depleted or natural uranium, but it is not possible to rule out enriched uranium.

### 3.3.3 Azimuthal Logging Data Analysis

The OU 7-13/14 project conducted azimuthal gamma-ray logging in selected probes within the DU Study Areas as a means to investigate the spatial distribution of subsurface radionuclides. Six probes were selected for the azimuthal surveys based on existing geophysical logging data. These probes were selected because they contained high levels of either  $^{238}\text{U}$  or  $^{237}\text{Np}$  (Table 3-14).

Azimuthal logging was conducted by GTS Duratek during May 2001, and preliminary results were delivered to the INEEL on May 31, 2001. Azimuthal logs were analyzed to choose probes for follow-up studies of  $^{238}\text{U}$  or  $^{237}\text{Np}$  leaching and migration. Azimuthal data were used to indicate the position of  $^{238}\text{U}$  or  $^{237}\text{Np}$  relative to the probe hole so that lysimeters could be installed to collect leachate samples.

For each probe, Table 3-15 lists detected radionuclides and gives the azimuth of the observed maximum count rate for each. Azimuth is measured with respect to a north arrow marked on the probe casing. Table 3-15 also gives the approximate maximum count rates and two general qualifiers. The first qualifier describes the statistical significance of the direction indication, and the second qualifier describes the narrowness of the direction indication (i.e. “good” indicates a highly directional source, and “poor” indicates a broadly directional source).

Table 3-14. Depleted Uranium Study Area probe holes selected for azimuthal logging.

Probe Hole	Depth (ft)	Radionuclide	Maximum cps <sup>a</sup>
DU-10	7.5	$^{238}\text{U}$	3,253
DU-16	11.5	$^{238}\text{U}$	6,604
DU-14	13.5	$^{238}\text{U}$	17,300
DU-03	8.0	$^{238}\text{U}$	1,979
DU-15	11.5	$^{238}\text{U}$	1,947
DU-08	14.5	$^{237}\text{Np}^{\text{b}}$	4,944

a. As observed by standard gamma-ray logging.

b.  $^{237}\text{Np}$  indicated by  $^{233}\text{Pa}$  daughter.

Table 3-15. Depleted Uranium Study Area azimuthal data summary.

Probe	Depth (ft)	Nuclide @ azimuth	Maximum cps	Statistics	Direction
DU-10	7.5	$^{238}\text{U}$ @ 190 degrees	4	Good	Good
DU-16	11.5	$^{238}\text{U}$ @ 135 degrees	2.5	Fair	Good
		$^{238}\text{U}$ @ 270 degrees	1.8	Good	Good
		2,614 keV @ 235 degrees	3.3	Good	Good
DU-16	13.5	$^{238}\text{U}$ @ 130 degrees	5.5	Good	Good
DU-14	8.0	$^{238}\text{U}$ @ 65 degrees	21	Good	Good
		$^{238}\text{U}$ @ 200 degrees	11	Good	Fair
DU-14	10.0	$^{238}\text{U}$ @ 190 degrees	1.1	Fair	Good
		$^{239}\text{Pu}$ @ 45 degrees	0.7	Fair	Good
DU-03	8.5	$^{238}\text{U}$ @ 140 degrees	1.4	Fair	Fair
DU-15	13.5	$^{239}\text{Pu}$ @ 315 degrees	75	Good	Good
DU-15	15.5	$^{238}\text{U}$ @ 35 degrees	1.7	Good	Good
DU-08	12.5	$^{238}\text{U}$ @ 350 degrees	0.5	Good	Good
DU-08	14.5	$^{233}\text{Pa}$ @ 190 degrees	14	Good	Good

### 3.3.4 Cluster Probe Analysis

Offset probes to Probe Hole DU-08 were installed to the south, approximately aligned with the high  $^{233}\text{Pa}$  direction as indicated by azimuthal logging (Figure 3-25). Logging data from the offset probes show the presence of  $^{233}\text{Pa}$ , most likely a continuation of the  $^{233}\text{Pa}$  source observed in DU-08 logging data. The three-probe pattern at this location is a good candidate for further study of the  $^{233}\text{Pa}$  source.

Offset probes to Probe Hole DU-10 were installed to the south-southwest, approximately aligned with the high  $^{238}\text{U}$  direction as indicated by azimuthal logging (Figure 3-26). Logging data from the offset probes show the presence of  $^{238}\text{U}$ , most likely a continuation of the  $^{238}\text{U}$  source observed in DU-10 logging data. The center of the  $^{238}\text{U}$  source appears to lie in the near vicinity of DU-10-B. The three-probe pattern at this location is a good candidate for further study of the  $^{238}\text{U}$  source.

Offset probes to Probe Hole DU-14 were installed to the northwest, approximately 100 degrees to the high  $^{238}\text{U}$  direction as indicated by azimuthal logging (Figure 3-27). Logging data from the offset probes show the presence of a weak  $^{238}\text{U}$  source, possibly a continuation of the  $^{238}\text{U}$  source observed in DU-08 logging data. The main body of the  $^{238}\text{U}$  source most likely does not occur within the area encompassed by the three probes. The three-probe pattern at this location is not a good candidate for further study of the  $^{238}\text{U}$  source.

# DU-08 OFFSET PROBES SUMMARY

Pa AZIMUTHAL LOG @ 14.5 FT  
SELECTED STANDARD LOGS

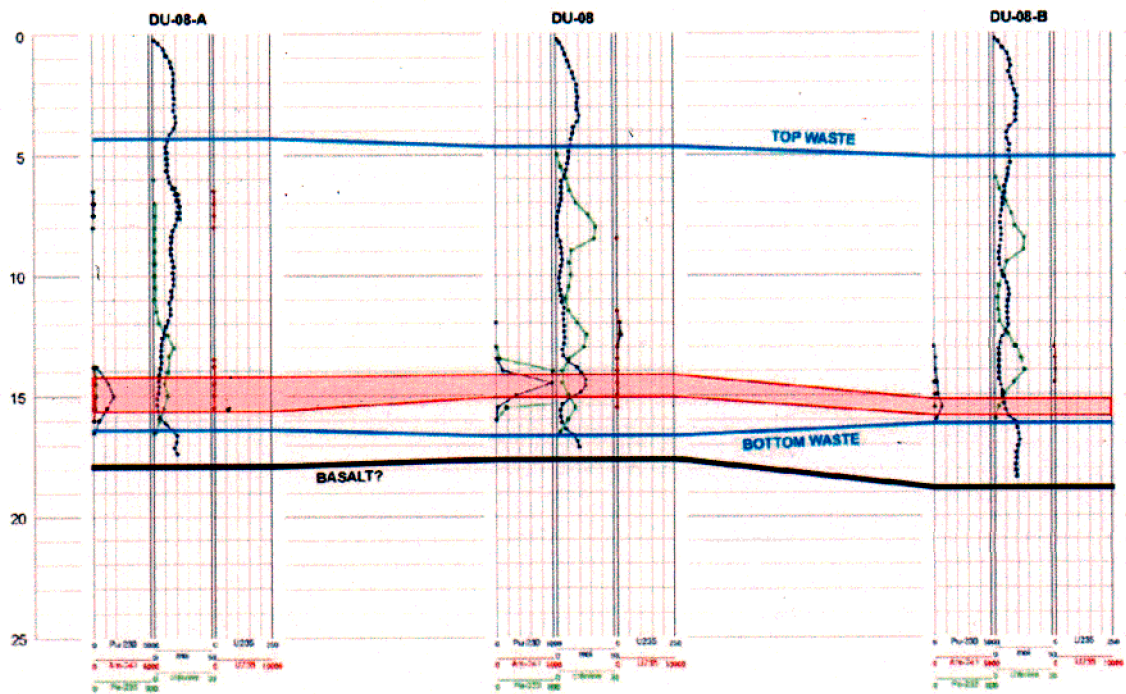
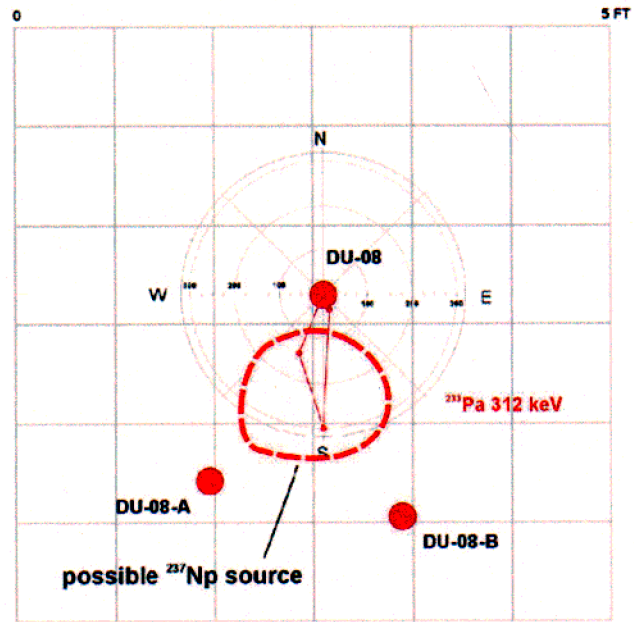


Figure 3-25. Cross section through partial probe cluster at Probe Hole Depleted Uranium-08.

# DU-10 OFFSET PROBES SUMMARY

<sup>238</sup>U AZIMUTHAL LOG @ 7.5 FT  
 SELECTED STANDARD LOGS

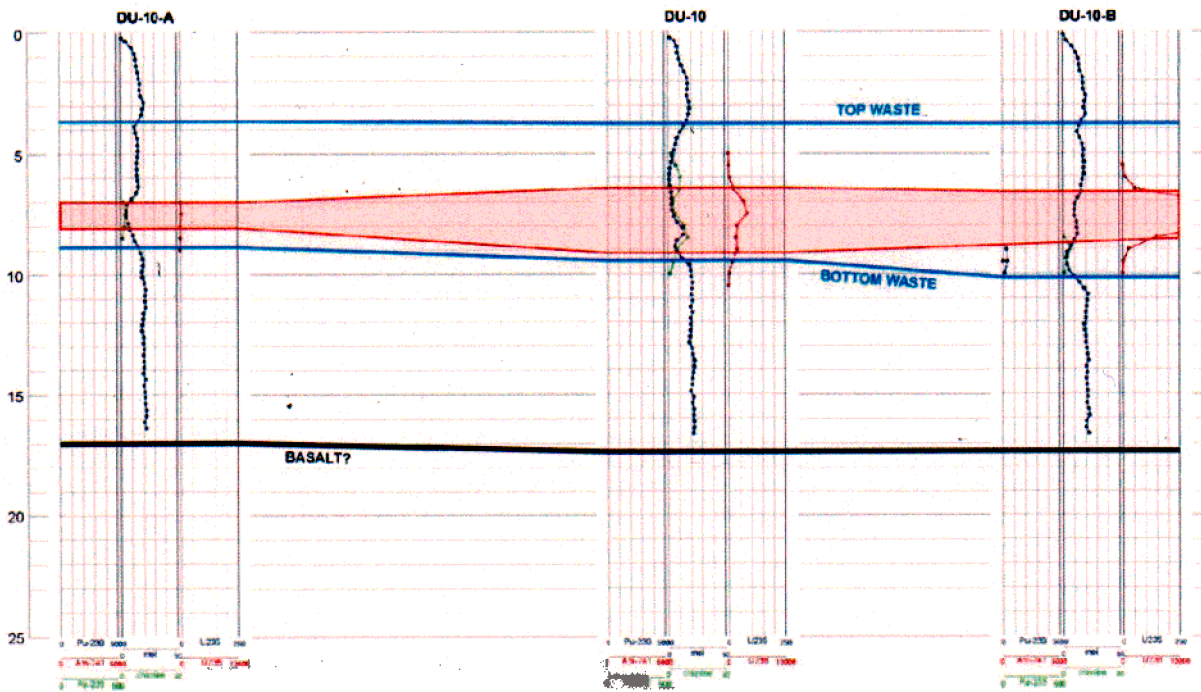
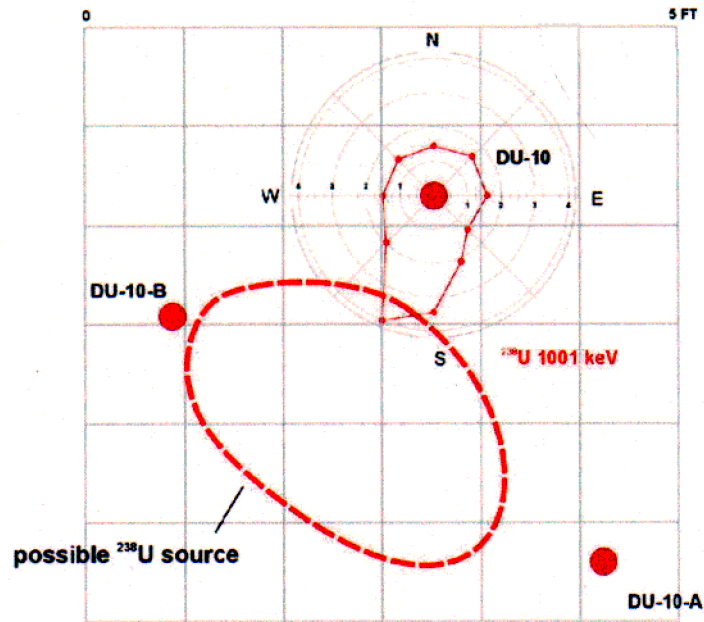


Figure 3-26. Cross section through partial probe cluster at Probe Hole Depleted Uranium-10.

# DU-14 OFFSET PROBE: SUMMARY

<sup>238</sup>U AZIMUTHAL LOG @ 8.0 FT  
SELECTED STANDARD LOGS

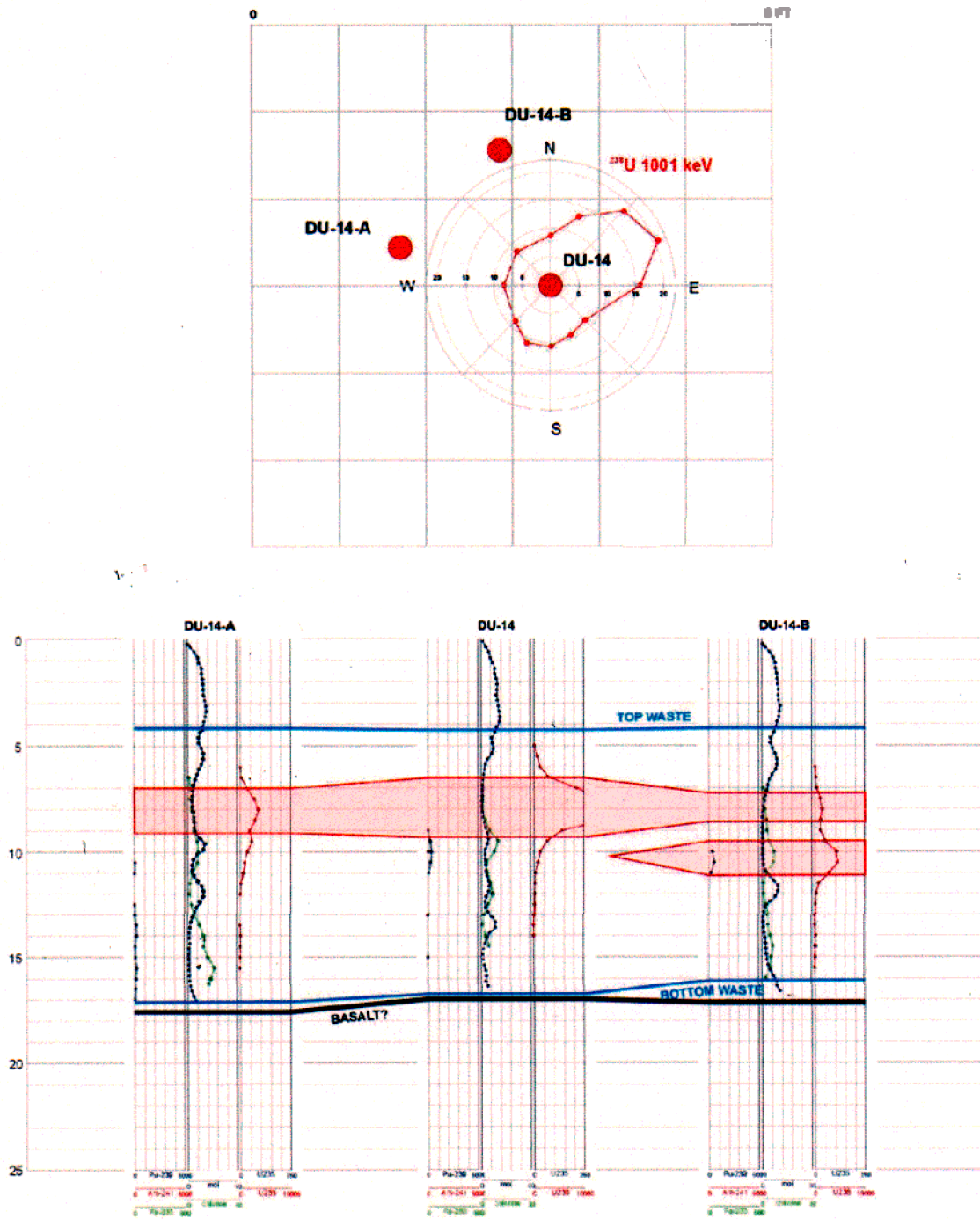


Figure 3-27. Cross section through partial probe cluster at Probe Hole Depleted Uranium-15.

### 3.4 Pit 5 Focus Area

The objective of the Pit 5 Focus Area investigation was to locate uranium-bearing waste shipments including suspected enriched uranium as indicated by inventory records.

#### 3.4.1 Selection of Probe Locations

Figure 3-28 shows surface geophysical data used for selecting probe locations in the Pit 5 Focus Area. Inventory data showed a concentration of RFP drums containing enriched uranium waste at two separate locations within Pit 5. Geophysical data were interpreted to indicate the location of concentrated metallic debris, such as 55-gal drums, in the vicinity of the targeted inventory. Accordingly, the Pit 5 Focus Area exploratory probes were arranged as profiles and positioned to intersect geophysical anomalies within the suspected drum areas. Figure 3-28 shows the final location of the Pit 5 Focus Area probes. The southern exploration area is referred to as Pit 5 Area 1, and the northern exploration area is referred to as Pit 5 Area 4.

#### 3.4.2 Observations on Radionuclide Contamination

The logging subcontractor conducted preliminary processing of the Pit 5 Study Area logging data. Their processing included automated spectral analysis of passive gamma-ray data to identify the presence of specific target contaminants including  $^{235}\text{U}$ ,  $^{238}\text{U}$ ,  $^{239}\text{Pu}$ ,  $^{241}\text{Am}$ , and  $^{237}\text{Np}$ . After applying a standard calibration correction to convert net count rates to apparent radionuclide concentrations, summary results were compiled and delivered to the INEEL along with the raw spectral data.

Table 3-16 gives maximum detected levels of key target contaminants for all Pit 5 Focus Area probes. Blank cells indicate nondetects.

Table 3-16. Radionuclide detection summary for the Pit 5 Focus Area.

Well ID	Gross Count Rate	$^{235}\text{U}$ (pCi/g) <sup>a</sup>	$^{238}\text{U}$ (pCi/g) <sup>a</sup>	$^{239}\text{Pu}$ (nCi/g) <sup>a</sup>	$^{233}\text{Pa}$ (pCi/g) <sup>a</sup>	$^{241}\text{Am}$ (nCi/g) <sup>a</sup>	$^{137}\text{Cs}$ (pCi/g) <sup>a</sup>	$^{60}\text{Co}$ (pCi/g) <sup>a</sup>	Cl_1165 (cps)
P5-01-01	345	ND	ND	ND	ND	ND	0.6	ND	ND
P5-01-02	410	ND	ND	ND	0.4	ND	0.5	ND	ND
P5-01-03	634	ND	ND	ND	ND	ND	0.3	ND	ND
P5-01-04	341	ND	ND	ND	ND	ND	0.2	ND	5.2
P5-01-05	ND	ND	ND	ND	ND	ND	ND	ND	ND
P5-01-06	392	ND	ND	42.1	ND	ND	0.1	ND	1.9
P5-01-07	3024	ND	ND	274.1	35.9	1,644.0	ND	ND	0.3
P5-01-08	29,452	ND	105.1	235.8	ND	ND	ND	ND	2.9
P5-04-01	11,336	14.1	10,947.0	12,653.0	95.4	3,246.0	71.7	13.7	8.0
P5-04-02	1,640	5.9	319.8	796.7	8.6	312.3	47.4	ND	2.7
P5-04-03	1,807	22.4	1,415.0	918.7	12.3	306.1	16.9	ND	9.8
P5-04-04	7,674	ND	7,038.0	271.8	ND	289.3	2.7	ND	2.2
P5-04-05	51,864	183.2	64,581.0	ND	ND	653.1	ND	ND	2.0
P5-04-06	10,069	ND	141.2	2,184.0	188.9	5,279.0	48.7	ND	3.7
P5-04-07	2,890	30.6	1,769.0	753.4	ND	2,543.0	23.5	ND	8.1

a. Assumes homogenous, isotropic, and unconsolidated soil media.  
ND = nondetect

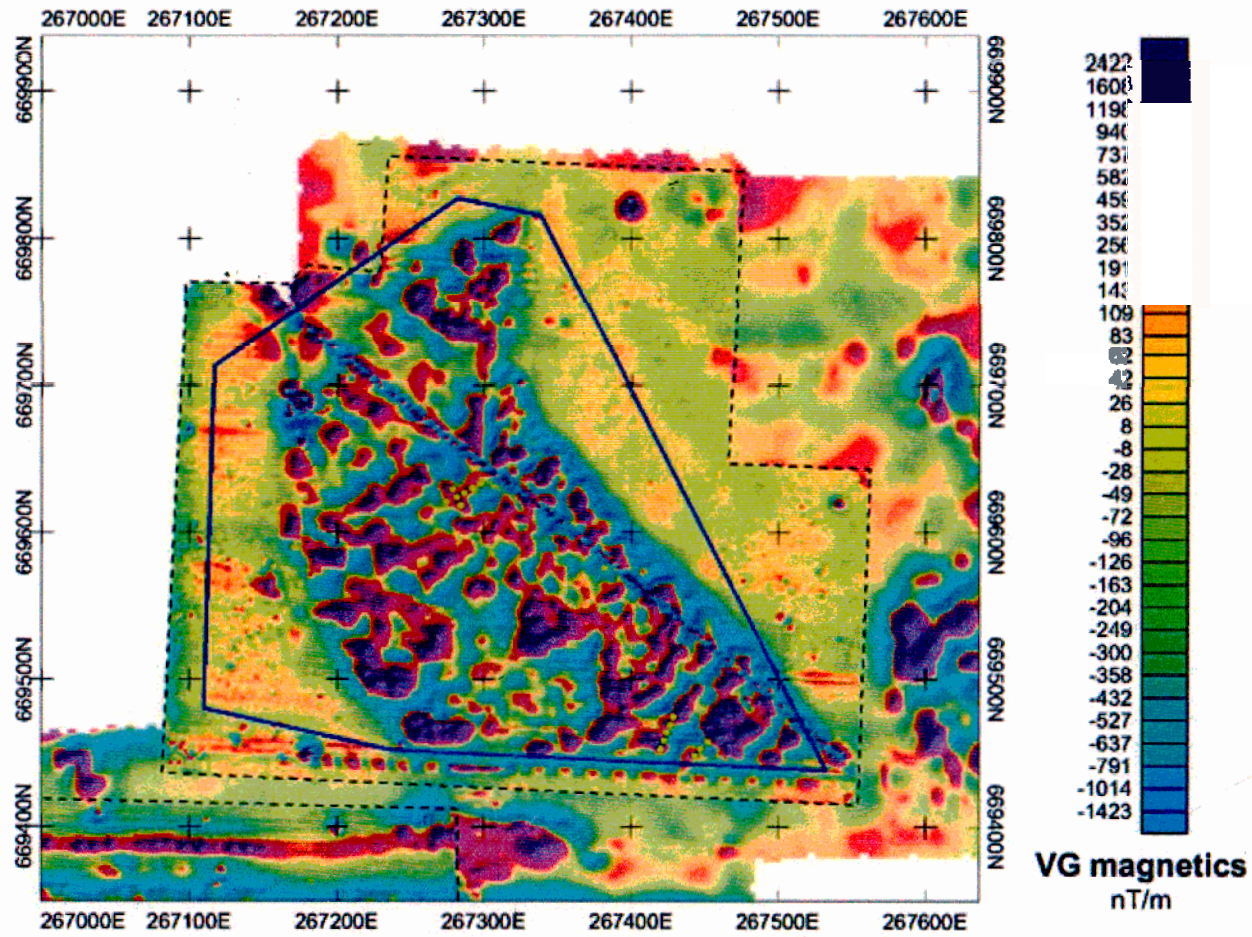


Figure 3-28. Surface geophysics for the Pit 5 Focus Area. Final probe locations are also shown.

Figures 3-29 and 3-30 give a summary of Pit 5 Area 1 and Area 2 logging results. These graphics show the spatial distribution and maximum apparent concentration of principal contaminants within these areas. Superimposed geophysical data reflect the distribution of buried metallic waste. Markers show the historical disposal location of targeted Rocky Flats shipments.

Figure 3-29 depicts the relative scarcity of radionuclide contamination in Pit 5 Area 1. The shipments targeted for investigation included 370 waste drums, 42 of which were reported to contain  $^{233}\text{U}$ . The  $^{233}\text{U}$  detection limit is estimated to be approximately 8 nCi/g using the 317 keV gamma ray, which means that  $^{233}\text{U}$  cannot be detected at the low levels possible for other uranium isotopes. Subcontractor analysis did not identify the 317 keV gamma ray above background in any of the Area 1 probe holes. Several P5-01-08 raw spectra were reexamined using INEEL analysis programs and confirmed this negative result.

Probe P5-01-08 had highly elevated 583 keV and 2614 keV gamma rays. One possible source of these gamma rays is  $^{232}\text{U}$ , which decays through  $^{232}\text{Th}$  to  $^{208}\text{Pb}$ .  $^{232}\text{U}$  is often found in combination with  $^{233}\text{U}$ . The elevated 583 keV and 2614 keV gamma rays may, therefore, be construed as indirect evidence for  $^{233}\text{U}$ , although other interpretations are possible.

Figure 3-30 shows the widespread presence of U, Pu, Am, Np, and chlorine contamination zones in Pit 5 Area 4. The shipments targeted for investigation in this area included 147 drums reported to contain primarily uranium waste. Fourteen of these drums were listed as containing highly enriched uranyl nitrate. Apparent radionuclide contamination levels range from low to moderate except for P5-04-05, which shows  $^{238}\text{U}$  at an apparent concentration of 64,581 pCi/g.

**3.4.2.1 Plutonium, Americium, and Neptunium.** Pu:Am and Am:Np apparent activity ratios for Pit 5 probes are shown in Figure 3-31. Computed ratios assume homogenous conditions and do not account for differential attenuation of gamma rays.

Table 3-17 shows a comparison between expected and observed Pu, Am, and Np ratios where the expected values are based on 30-year decay of weapons-grade plutonium. The Am:Np ratio suggests an excess of Np relative to the amount expected from pure Am decay.

**3.4.2.2 Uranium-235 and Uranium-238.** Figure 3-31 shows  $^{238}\text{U}$ : $^{235}\text{U}$  apparent activity ratios for the Pit 5 probes. Computed ratios assume homogenous conditions and do not account for differential attenuation of gamma rays.

Weight ratios  $^{235}\text{U}$ : $^{238}\text{U}$  were computed for all logging stations having valid measurements for both  $^{235}\text{U}$  and  $^{238}\text{U}$  (Table 3-18). The computed ratios assume the uranium isotopes to be uniformly co-located beginning immediately outside the probe casing. Ratios range from 0.1–0.5%, suggesting depleted uranium. It is important to note that differential attenuation of the  $^{235}\text{U}$  186 keV gamma ray relative to the  $^{238}\text{U}$  1,001 keV gamma ray can cause errors in the computed ratios when the isotopes are not co-located or occur more than a few centimeters from the casing. Nonetheless, it is unlikely that the detected uranium contamination zones encompass highly enriched uranyl nitrate (expected  $^{235}\text{U}$ : $^{238}\text{U}$  > 90.0%).

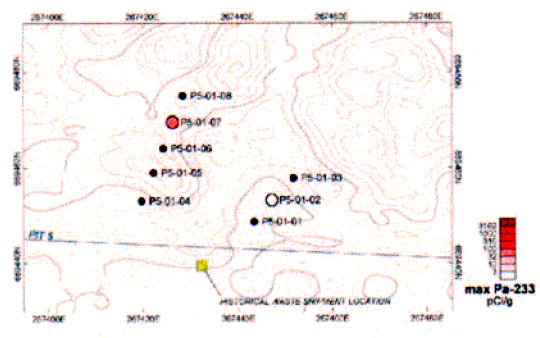
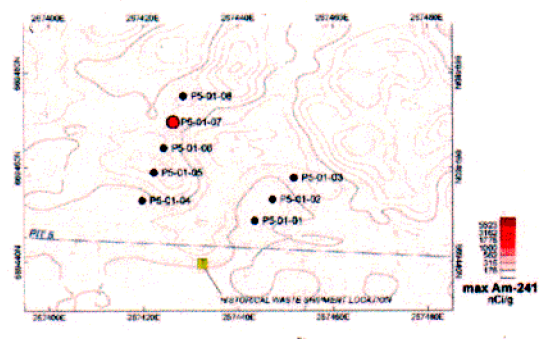
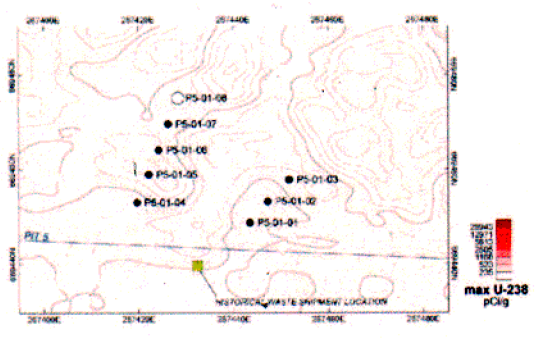
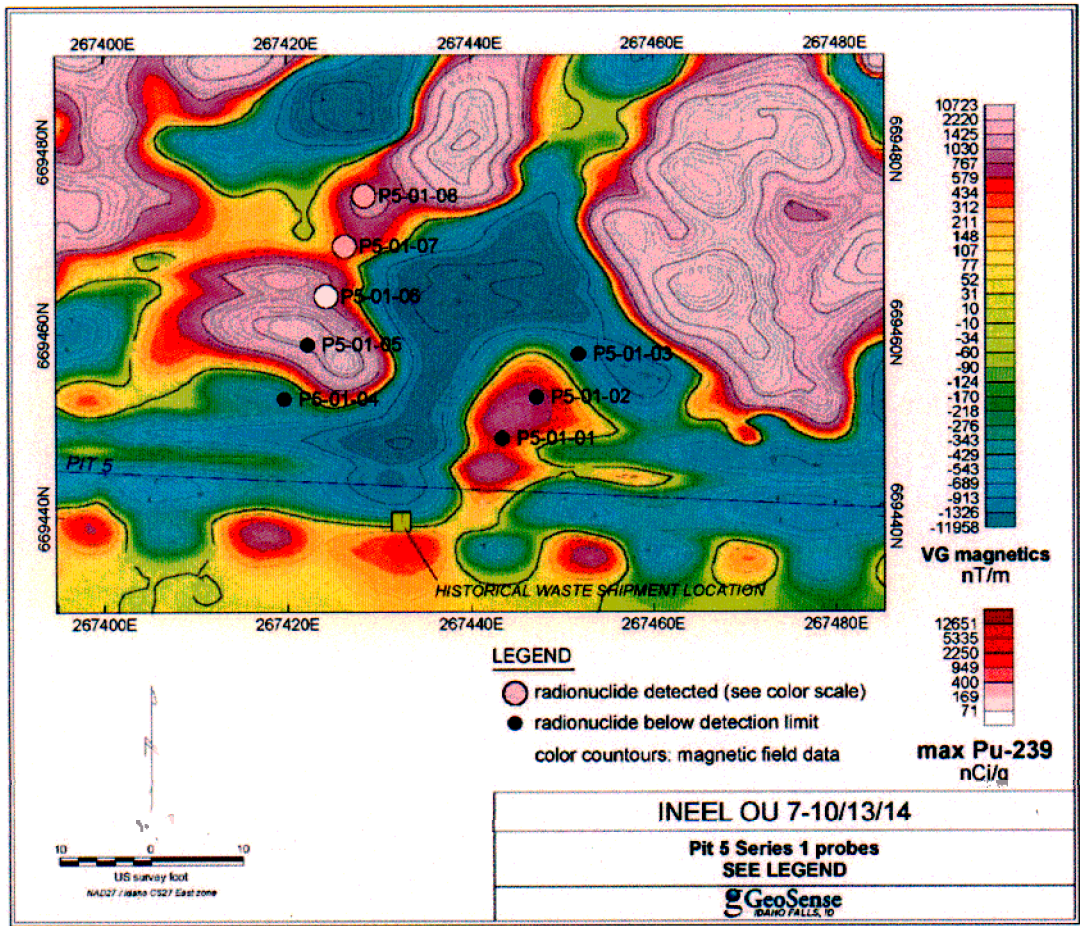


Figure 3-29. Logging results summary for the Pit 5 Focus Area, Series-1 probes.

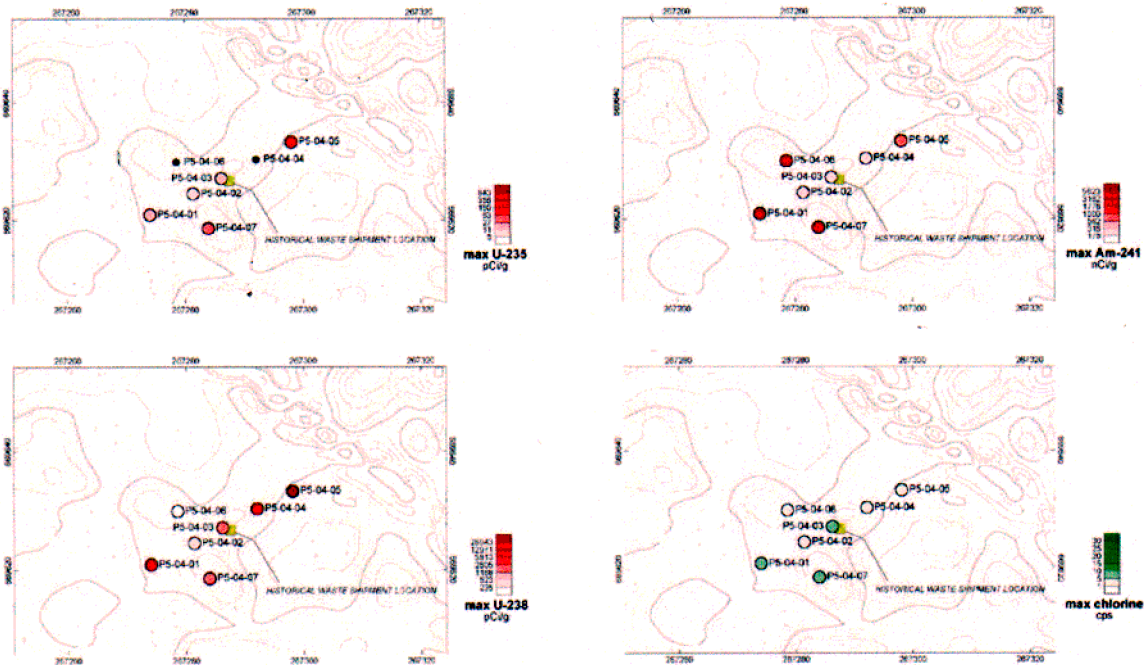
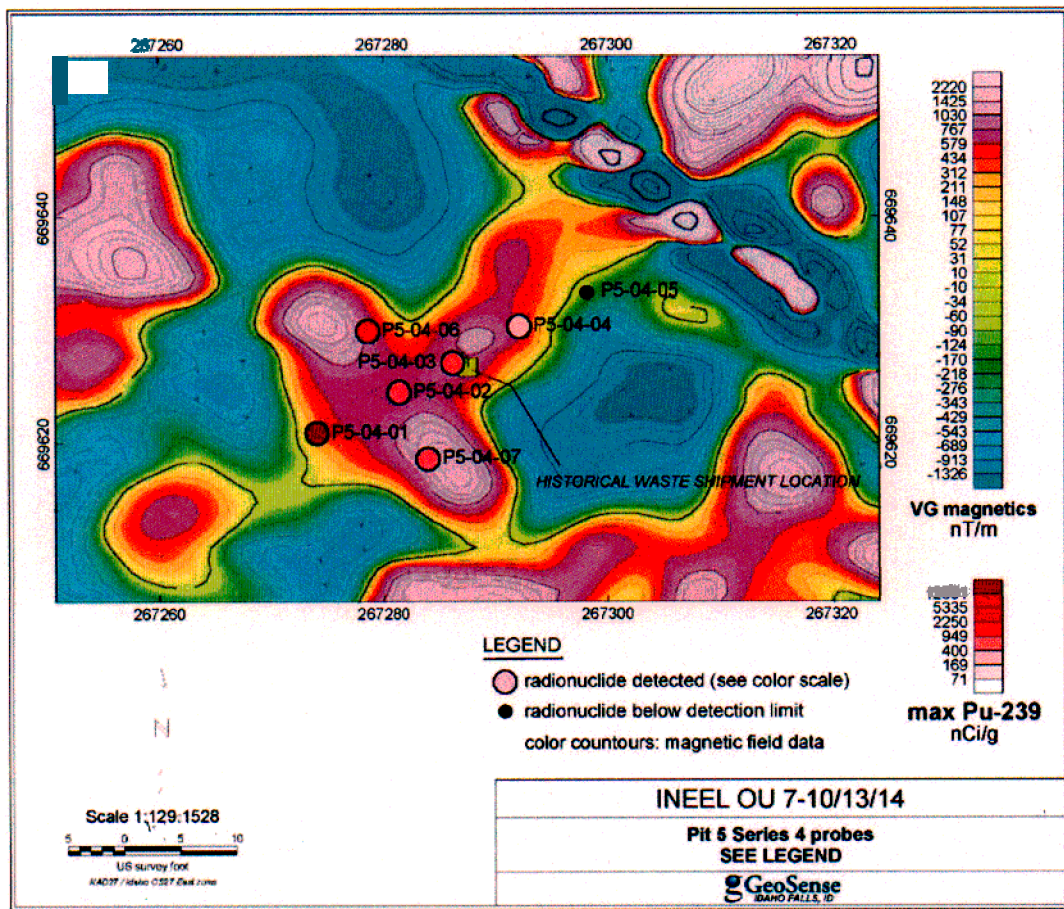


Figure 3-30. Logging results summary for the Pit 5 Focus Area, Series-4 probes.

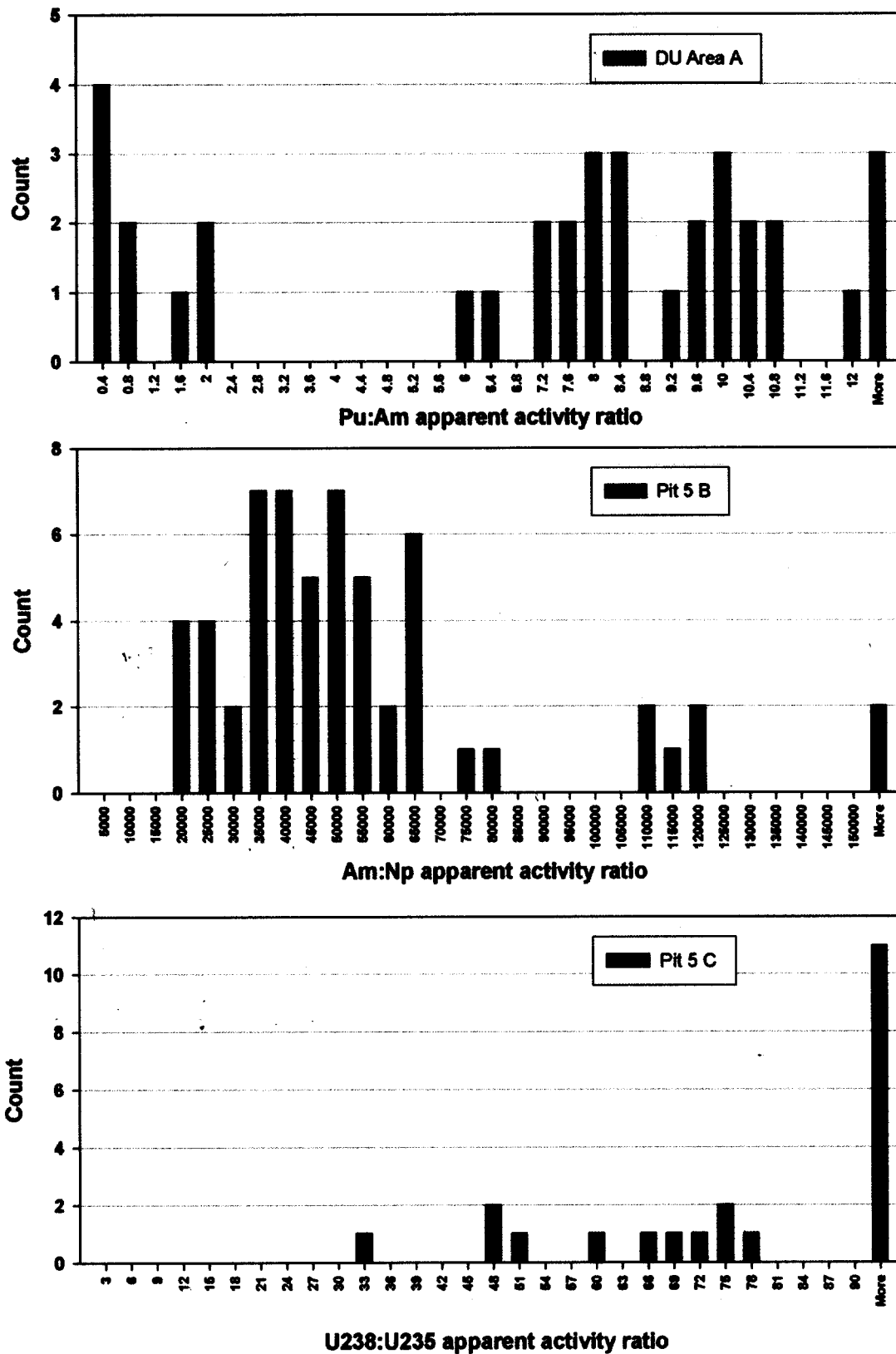


Figure 3-31. Histogram of isotopic ratios for the Pit 5 Study Area probes.

Table 3-17. Comparison of expected and observed Pu, Am, and Np activity ratios.

Ratio	Weapons-Grade Plutonium	Observed
$^{239}\text{Pu}:$ $^{241}\text{Am}$	6.7	7–11
$^{241}\text{Am}:$ $^{237}\text{Np}$	100,000	20,000–65,000

Table 3-18. Pit 5 Area 4 apparent  $^{235}\text{U}:$  $^{238}\text{U}$  ratios (by weight).

Well ID	Depth	$^{235}\text{U}_{186}$	$^{238}\text{U}_{1,001}$	Ratio (%)
P5-04-03	9.00	4.25	136.4	0.484
P5-04-03	9.50	2.14	98.86	0.336
P5-04-07	6.50	7.65	357.4	0.332
P5-04-02	12.50	5.87	289.1	0.315
P5-04-07	8.50	30.55	1,769	0.268
P5-04-03	6.50	22.37	1,415	0.246
P5-04-03	7.00	15.0	1,005	0.232
P5-04-03	6.00	18.79	1,316	0.222
P5-04-07	8.00	23.63	1,708	0.215
P5-04-07	6.00	3.59	264.5	0.211
P5-04-03	7.50	6.3	476.2	0.206
P5-04-03	5.50	6.91	625.7	0.172
P5-04-07	7.00	3.51	371.6	0.147
P5-04-05	9.96	96.13	10,291	0.145
P5-04-07	9.00	5.56	610.4	0.141
P5-04-05	9.00	68.89	8,372	0.128
P5-04-05	9.50	24.72	3,744	0.103
P5-04-05	8.50	130.8	21,059	0.096
P5-04-07	9.50	1.04	178.8	0.090
P5-04-05	8.00	183.2	52,951	0.054
P5-04-05	7.00	87.74	64,581	0.021
P5-04-01	7.00	14.11	10,947	0.020
P5-01-01	0.00	1.0	150	0.104

**3.4.2.3 Uranium-233 Detection Limit.** Although  $^{233}\text{U}$  has a long half-life ( $1.592 \times 10^5$  yr) and the specific activity is low (0.00964 Ci/g), it does emit a large number of gamma rays with branching ratios comparable to the gamma-ray emissions of  $^{239}\text{Pu}$ . Table 3-19 compares attributes of the  $^{233}\text{U}$  317-keV gamma ray to those of the  $^{239}\text{Pu}$  414-keV gamma ray and shows that the  $^{233}\text{U}$  gamma activity at 317 keV is 91% of the  $^{239}\text{Pu}$  gamma activity at 414 keV.

The five most prominent  $^{233}\text{U}$  gamma rays (in terms of branching ratio) within the calibration limits of the GTS Duratek system are, in descending order: 317 keV, 164 keV, 291 keV, 245 keV, and 217 keV. From this list, the 317-keV gamma ray was selected as the primary gamma. Consideration was then given to potential interference from naturally-occurring radionuclides and other anthropogenic radionuclides (i.e.,  $^{233}\text{Pa}$ ,  $^{239}\text{Pu}$ , and  $^{241}\text{Am}$ ). Both  $^{241}\text{Am}$  and  $^{233}\text{Pa}$  emit gamma rays at 312 keV; however, interference with the 317 keV should be minimal due to the 5-keV energy difference. The logging system should have sufficient resolution to resolve these two peaks.

The minimum detected concentration of  $^{239}\text{Pu}$  in all SDA probe holes was 7 nCi/g in Probe Hole P9-16 (based on less than 30% counting uncertainty). A rough estimate as to the minimum detectable concentration of  $^{233}\text{U}$ , assuming 30% counting uncertainty, is 8 nCi/g.

Table 3-19. Comparison between  $^{233}\text{U}$  and  $^{239}\text{Pu}$  gamma-ray attributes.

Attribute	$^{233}\text{U}$	$^{239}\text{Pu}$
Gamma-ray energy	317 keV	414 keV
Gamma-ray intensity	$3.139 \times 10^4$ $\gamma$ /s/g	$3.466 \times 10^4$ $\gamma$ /s/g
Half-life	$1.592 \times 10^5$ yr	$2.41 \times 10^4$ yr
Specific activity	$9.6 \times 10^{-3}$ Ci/g	$6.2 \times 10^{-2}$ Ci/g
Relative activity	91%	100%

## 3.5 Pit 9 Study Area and Pit 9 Campaign 1

The Pit 9 Study Area and Pit 9 Campaign 1 were investigated under the OU 7-10 Staged Interim Action Project. Logging results for these studies are discussed extensively in three documents (Josten and Okeson 2000; Okeson 2000; Beitel, Kuan, Bishop, and Josten 2000). Briefly, the OU 7-10 project objective was to identify a small area within Pit 9 containing RFP waste. An initial investigation area was selected using inventory records and surface geophysical data. Probes were then installed to facilitate downhole logging. Downhole logging data were then used to select a small area suitable for a limited waste retrieval project.

### 3.5.1 Selection of Probe Locations

Figure 3-32 shows surface geophysical data used for selecting probe locations in the Pit 9 Study Area and Pit 9 Campaign 1. Waste inventory data showed a high concentration of drums containing RFP sludge and combustible and noncombustible waste throughout the southern end of Pit 9. Geophysical data support the interpretation of large irregularly shaped waste blocks that appear to have higher concentrations of buried metal than adjacent areas. A symmetric probing pattern consisting of 20 (P9-01–P9-20) probes was developed to sample a 40 × 40-ft portion of Pit 9, referred to as the Pit 9 Study Area. Under Pit 9 Campaign 1, eight additional probes (P9-21A–P9-28A) were installed north of the original 20 probes to extend the area of investigation. Figure 3-32 shows the final location of the Pit 9 Study Area and Pit 9 Campaign 1 probes.

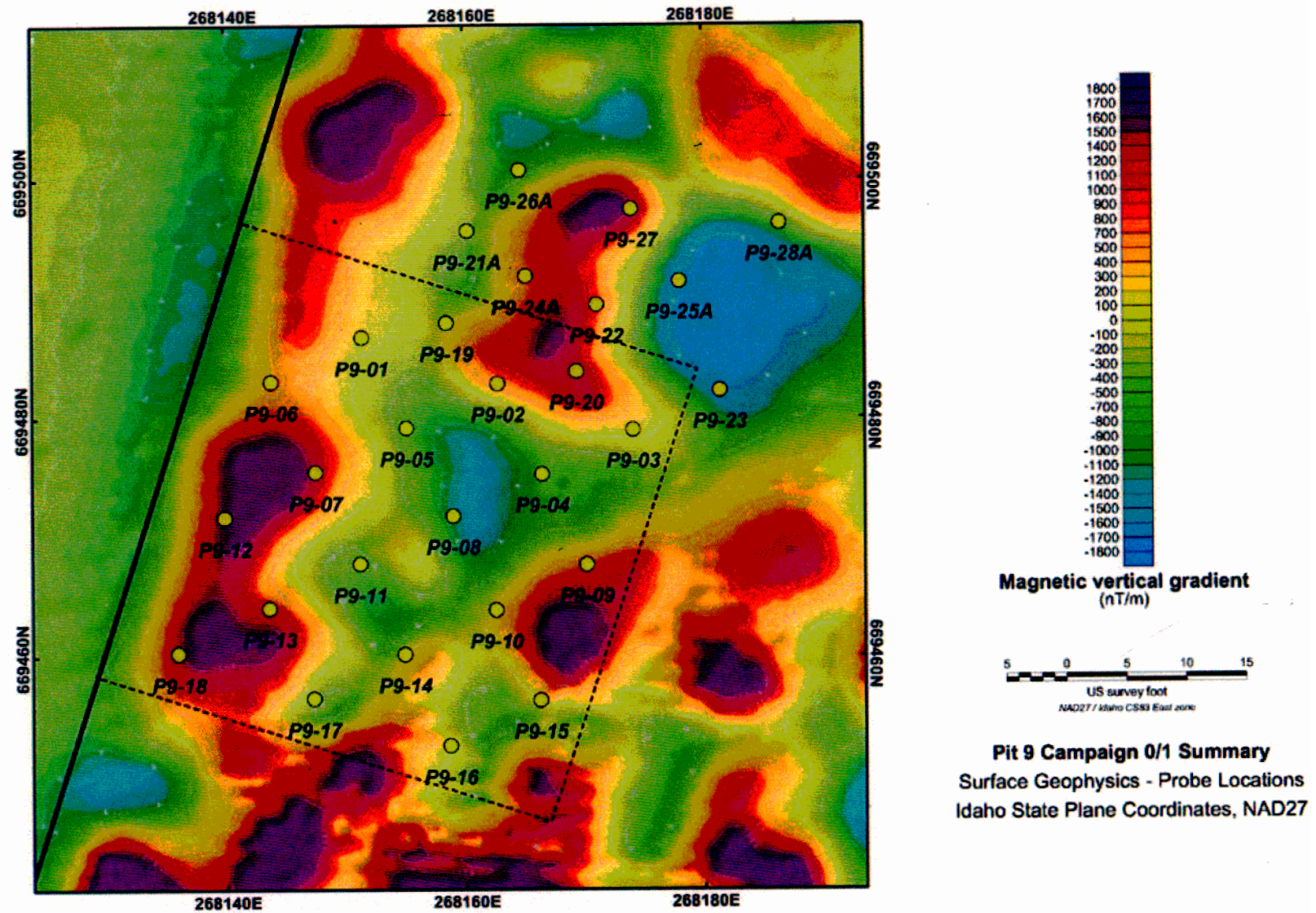


Figure 3-32. Surface geophysics for the Pit 9 Study Area and Pit 9 Campaign 1. Final probe locations are shown.

### 3.5.2 Observations on Radionuclide Contamination

The logging subcontractor conducted preliminary processing of the Pit 9 Study Area and Pit 9 Campaign 1 logging data. Their processing included automated spectral analysis of passive gamma-ray data to identify the presence of specific target contaminants including  $^{235}\text{U}$ ,  $^{238}\text{U}$ ,  $^{239}\text{Pu}$ ,  $^{241}\text{Am}$ , and  $^{237}\text{Np}$ . After applying a standard calibration correction to convert net count rates to apparent radionuclide concentrations, summary results were compiled and delivered to the INEEL along with the raw spectral data.

Table 3-20 gives maximum detected levels of key target contaminants for all Pit 9 Study Area and Pit 9 Campaign 1 probes. Blank cells indicate nondetects.

The Pit 9 Study Area was explored by 20 probes ranging in depth from 9 to 18 ft. Pu and Am contamination is observed primarily in the eastern portion of the study area with very high Pu radiation levels measured in Probe Hole P9-20. The high radiation levels in this probe hole were confirmed by repeat logging. Chlorine contamination is widespread but at generally lower (apparent) levels than seen at Pits 4 and 10. Uranium contamination is also widespread.

The Campaign 1 Study Area, located immediately north of the Pit 9 Study Area, was explored by eight probe holes ranging in depth from 10 to 12 ft. The eight probe holes showed similar characteristics to the eastern Pit 9 Study Area probe holes with both Pu and Am contamination and low-level (apparent) chlorine. No uranium was detected.

**3.5.2.1 Plutonium, Americium, and Neptunium.** Pu:Am and Am:Np apparent activity ratios for the Pit 9 Study Area and Pit 9 Campaign 1 probes are shown in Figure 3-33. Computed ratios assume homogenous conditions and do not account for differential attenuation of gamma rays.

Table 3-21 shows a comparison between expected and observed Pu, Am, and Np ratios where the expected values are based on 30-year decay of weapons-grade plutonium. The Am:Np ratio suggests an excess of Np relative to the amount expected from pure Am decay.

**3.5.2.2 Uranium-235 and Uranium-238.** Figure 3-33 shows  $^{238}\text{U}$ : $^{235}\text{U}$  apparent activity ratios for DU Study Area probes. Computed ratios assume homogenous conditions and do not account for differential attenuation of gamma rays.

### 3.5.3 Azimuthal Logging Data Analysis

Pit 9 Study Area azimuthal logging was conducted under the OU 7-10 project and is discussed in two reports (Josten and Okeson 2000; Okeson 2000). Figure 3-34 shows a preliminary compilation of azimuthal logging results.

### 3.5.4 Cluster Probe Analysis

A six probe cluster was installed surrounding Probe Hole P9-20 to facilitate detailed analysis of the  $^{239}\text{Pu}$  source near this probe. Figure 3-35 presents a summary of  $^{239}\text{Pu}$  passive gamma-ray and azimuthal gamma-ray logging data for the P9-20 cluster probes at 6-ft depth. These data sets suggest that the original P9-20 probe penetrated a  $^{239}\text{Pu}$  contaminated drum. The center of this drum lies approximately 1 ft south of P9-20. The source drum probably does not extend all the way to P9-20-01, which is the next closest probe to the  $^{239}\text{Pu}$  source at 6 ft. Key evidence for this interpretation includes the significantly lower 414 keV passive gamma-ray levels in the surrounding probes and the convergence of the azimuthal pointers toward a source south of P9-20.

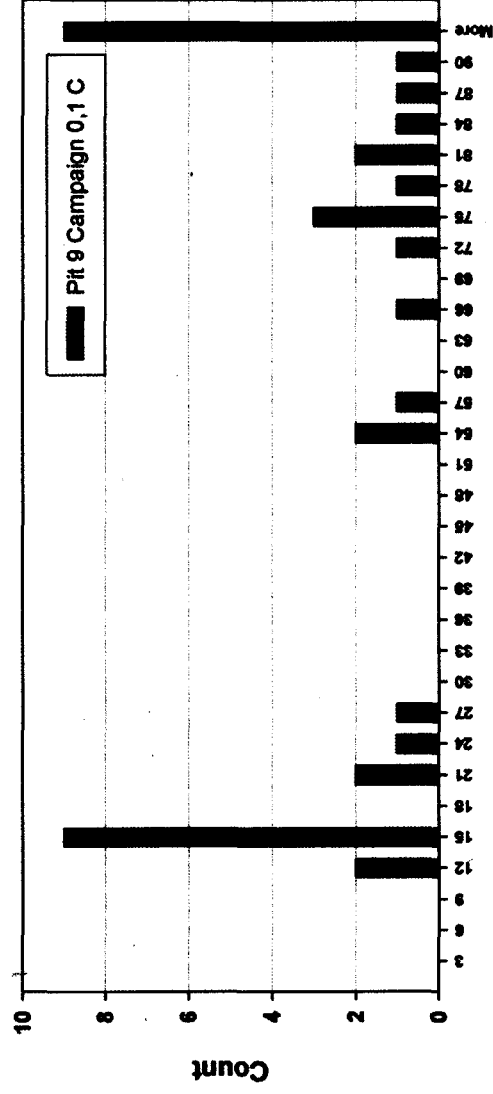
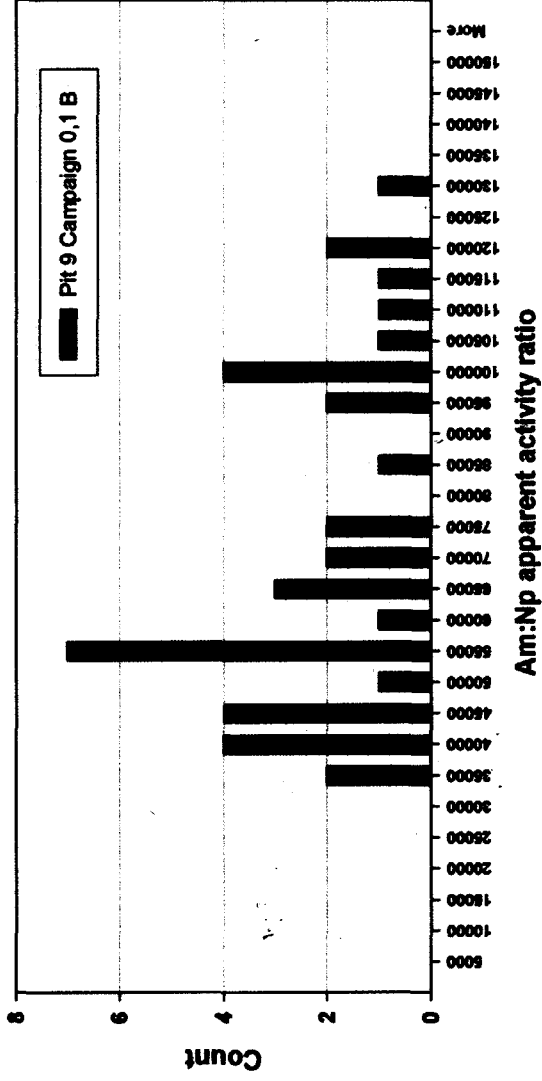
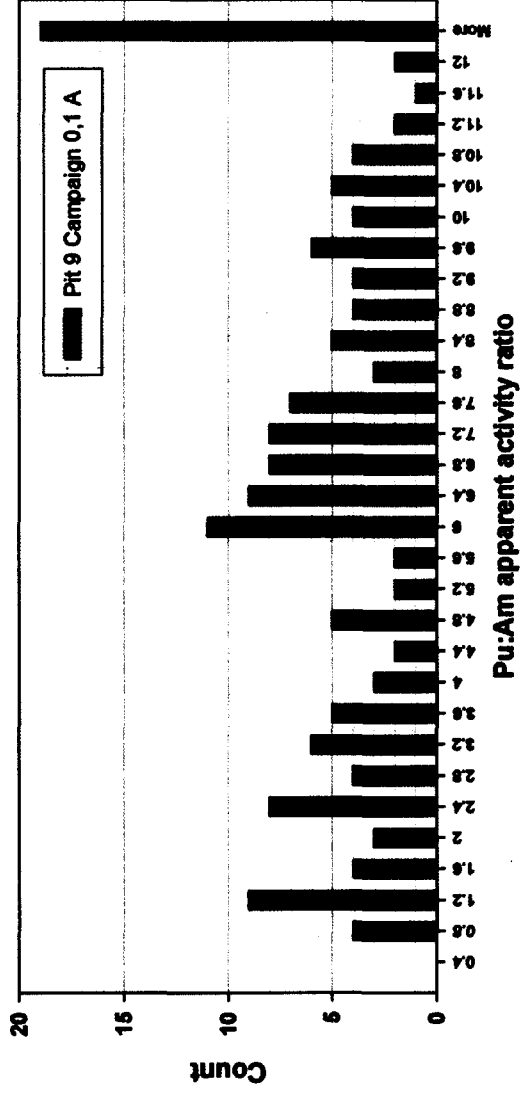
Table 3-20. Maximum apparent concentration values for Pit 9 Study Area and Pit 9 Campaign 1 probes.

Well ID	Gross Count Rate	<sup>235</sup> U (pCi/g) <sup>a</sup>	<sup>238</sup> U (pCi/g) <sup>a</sup>	<sup>239</sup> Pu (nCi/g) <sup>a</sup>	<sup>233</sup> Pa (pCi/g) <sup>a</sup>	<sup>241</sup> Am (nCi/g) <sup>a</sup>	<sup>137</sup> Cs (pCi/g) <sup>a</sup>	<sup>60</sup> Co (pCi/g) <sup>a</sup>	Cl_1165 (cps)
P9-01	402	ND	24.0	280.4	ND	ND	0.7	ND	7.1
P9-02	637	ND	69.6	308.1	ND	ND	ND	ND	1.3
P9-03	1,925	ND	37.2	1,598.0	ND	ND	ND	ND	38.0
P9-04	419	ND	ND	308.9	ND	ND	ND	ND	8.3
P9-05	278	ND	ND	33.8	19.8	ND	ND	ND	2.0
P9-06	432	ND	361.0	151.7	ND	ND	0.6	ND	19.8
P9-07	216	ND	ND	ND	ND	ND	0.6	ND	4.3
P9-08	1,822	33.9	2,516.0	ND	ND	ND	0.4	ND	6.9
P9-09	1,430	ND	385.9	696.3	ND	274.0	ND	ND	16.9
P9-10	295	ND	ND	ND	ND	ND	0.7	ND	3.0
P9-11	554	30.3	387.0	36.2	ND	ND	0.7	ND	4.6
P9-12	213	ND	ND	ND	ND	ND	ND	ND	6.9
P9-13	209	ND	68.8	ND	ND	ND	ND	ND	14.9
P9-14	265	ND	ND	36.2	ND	ND	0.5	ND	3.2
P9-15	603	ND	ND	484.8	ND	56.9	ND	ND	3.3
P9-16	244	ND	ND	72.5	ND	ND	0.4	ND	16.7
P9-17	239	ND	66.9	ND	ND	ND	0.7	ND	5.7
P9-18	211	ND	27.0	ND	ND	ND	0.3	ND	12.0
P9-19	440	5.4	296.0	18.6	ND	ND	ND	ND	10.8
P9-20	257,877	ND	ND	194,171.0	ND	20,770.0	ND	ND	3.4
P9-20-01	47,990	ND	ND	41,181.0	111.4	4,557.0	ND	ND	3.1
P9-20-02	22,115	ND	ND	6,562.0	157.9	12,663.0	ND	ND	3.1
P9-20-03	11,865	ND	ND	5,926.0	19.6	861.0	ND	ND	2.2
P9-20-04	962	ND	62.4	477.6	ND	74.4	ND	ND	1.8
P9-20-05	5,966	ND	24.0	4,482.0	12.5	479.8	0.7	ND	1.3
P9-20-06	18,334	ND	ND	13,640.0	34.4	1,844.0	1.1	ND	16.6
P9-21A	362	ND	ND	128.2	ND	ND	0.7	ND	3.1
P9-22	1,693	ND	ND	1,499.0	ND	141.3	ND	ND	3.0
P9-23	316	ND	ND	91.5	ND	ND	1.6	ND	1.2
P9-24A	4,611	ND	ND	3,917.0	ND	664.4	ND	ND	5.4
P9-25A	1,168	ND	ND	952.1	ND	86.5	ND	ND	2.7
P9-26A	346	ND	ND	111.0	ND	ND	1.0	ND	0.8
P9-27	2,598	ND	ND	2,549.0	ND	235.1	ND	ND	5.9
P9-28A	225	ND	ND	ND	ND	ND	ND	ND	ND

a. Assumes homogenous, isotropic, and unconsolidated soil media.  
 ND = nondetect

Table 3-21. Comparison of expected and observed Pu, Am, and Np activity ratios.

Ratio	Weapons-Grade Plutonium	Observed
<sup>239</sup> Pu: <sup>241</sup> Am	6.7	1-12; >12
<sup>241</sup> Am: <sup>237</sup> Np	100,000	35,000-75,000; 95,000-120,000



**U238:U235 apparent activity ratio**  
 Figure 3-33. Histogram of isotopic ratios for Pit 9 Study Area and Pit 9 Campaign 1 probes.

# Pit 9 Study Area AZIMUTHAL LOGGING SUMMARY

## LEGEND

- ▼ Pu-239
- ▶ Cs-137? (662 keV)
- ▶ U-238

LENGTH OF  
ARROWS SHOWS RATIO:  $\frac{\text{MAX\_DIRECTION\_CPS}}{180\_DIRECTION\_CPS}$

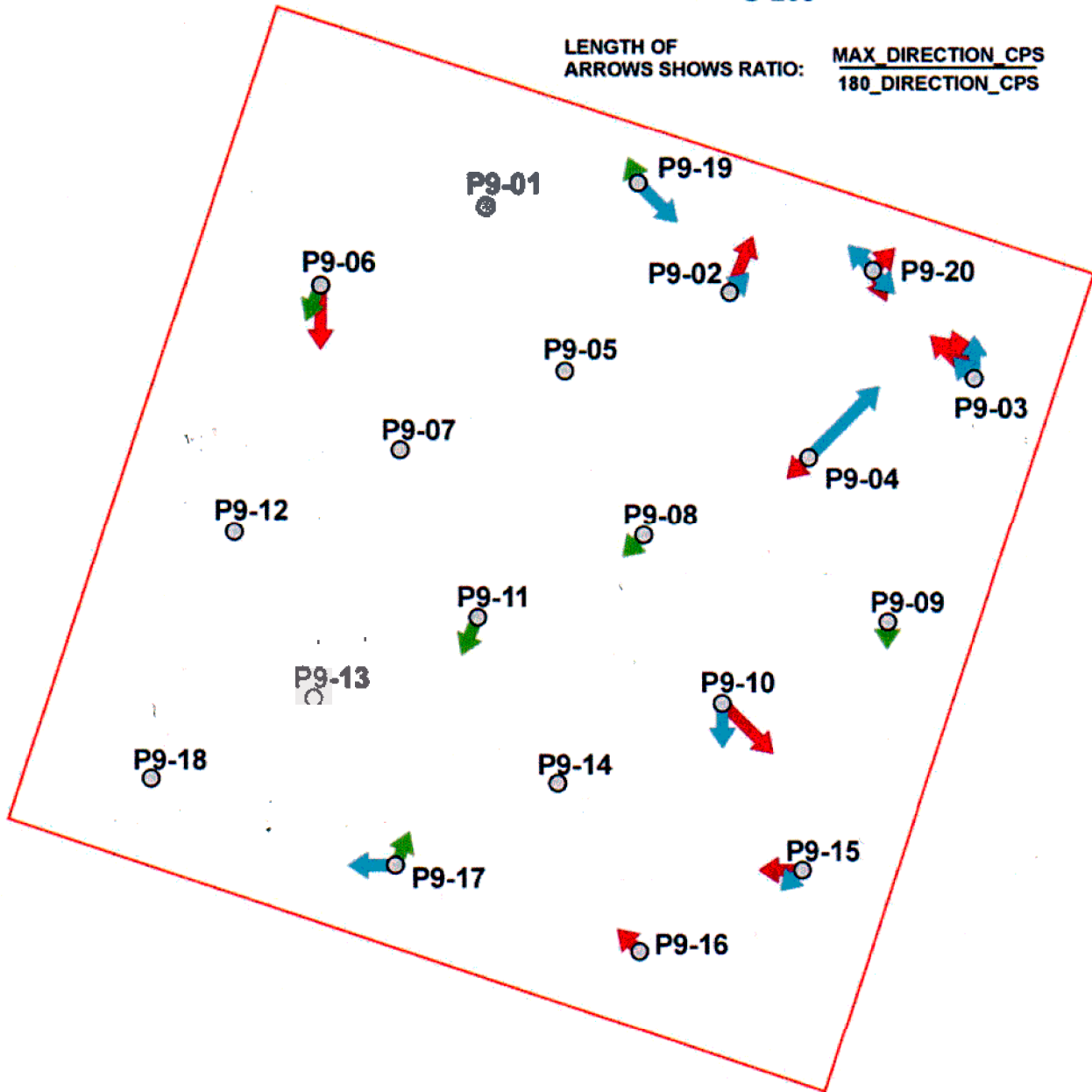


Figure 3-34. Azimuthal logging summary for Pit 9 Study Area probes.

## P9-20 cluster probe summary Pu-239 @ 6.0 ft

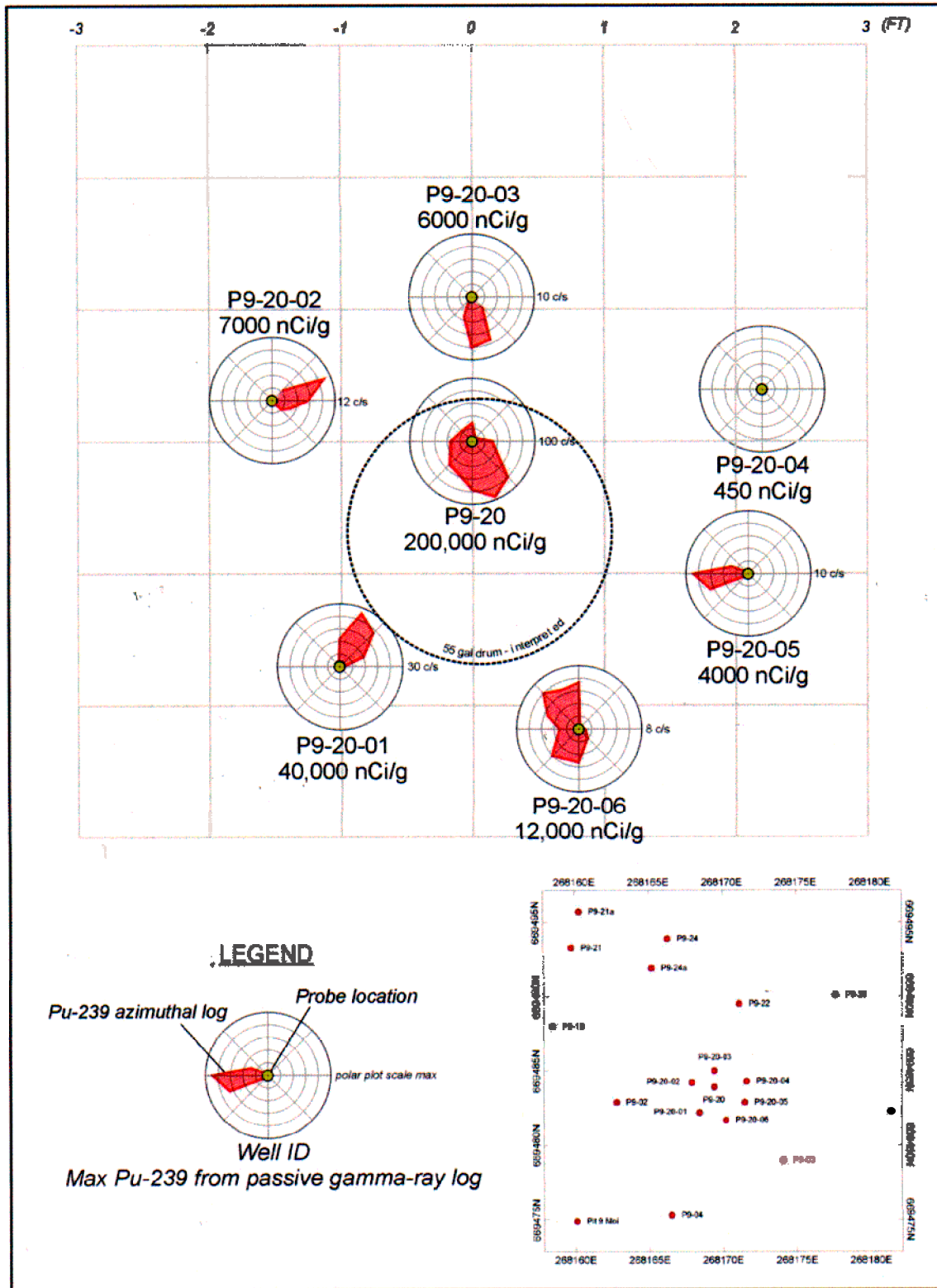


Figure 3-35. Azimuthal logging summary for the P9-20 probe cluster at 6 ft.

In contrast,  $^{239}\text{Pu}$  data for the 9–10-ft interval suggests small  $^{239}\text{Pu}$  sources with the predominant source occurring north of P9-20 (Figure 3-36). Probe P9-20-03 may possibly have penetrated a drum containing this  $^{239}\text{Pu}$  source.

Figure 3-37, a “spiral” cross section through the P9-20 cluster probes, depicts the depth relationship between the  $^{239}\text{Pu}$  sources. Extreme downward deflections of the Si/Ca/K40 curves are observed at 6 ft in P9-20 and at 8–9 ft in P9-20-03 (not shown). These deflections may reflect changes in the surrounding medium due to drum penetration.

## 3.6 Pit 9 Campaign 2

The Pit 9 Campaign 2 investigation was conducted under the OU 7-10 Staged Interim Action Project. The objective of this investigation was to explore for additional Pit 9 locations that could contain large  $^{239}\text{Pu}$  sources. Inventory records were used to identify waste forms that could contain concentrated  $^{239}\text{Pu}$  material. The locations of the targeted shipments, containing high-efficiency particulate air filters and graphite mold waste, were estimated based on surface geophysics data.

### 3.6.1 Selection of Probe Locations

Figure 3-38 shows surface geophysics and inventory information for Pit 9 Campaign 2 probe exploration. Fifteen probes were installed divided between two exploration areas believed to contain high Pu waste forms. The targets for the northern exploration area were high-efficiency particulate air filters disposed in cartons and/or wooden crates. The targets for the second exploration area were RFP drums containing graphite mold debris.

Key geophysical marker shipments in the vicinity of the targeted filter shipments were selected following review of the inventory records. Figure 3-38 (left panel) shows the interpreted locations for these marker shipments (geophysical highs annotated by lowercase letters) in comparison to the shipment positions defined by the inventory data (rectangles annotated by corresponding upper case letters). Note that the shipment labeled “A” consists of three separate PM2A skids, and the shipment labeled “F” consists of six separate equipment boxes arranged in two shipments. The location of these marker shipments as interpreted from the geophysical data defines a rough boundary around the targeted filter shipments. The filter shipments themselves are expected to have a diffuse geophysical signature that could include some local highs.

On the basis of these inferences, eight probe locations were proposed on two intersecting transects with a 10-ft spacing between probes. The proposed transect locations correspond to the target shipment positions as indicated in the inventory records. These locations have the expected geophysical character as it is currently understood and do not intersect any of the marker shipment locations.

The graphite shipments selected as potential exploration targets are highlighted in red in Figure 3-38 (right panel). The northern shipment located just above the Pit 9 dogleg contains five graphite drums out of 130 total drums. The shipment south of the dogleg along the eastern Pit 9 boundary contains 13 graphite drums out of 130 total drums. For both shipments, the odds for installing a probe within a foot or two of a graphite drum are poor.

The graphite drum shipments occur adjacent to many other RFP drum shipments and cannot be distinguished based on unique geophysical character. In addition to the drum shipments, inventory records show three small metal scrap shipments near the southern graphite shipment. These scrap shipments further complicate the problem of associating geophysical anomalies with specific shipments.

## P9-20 cluster probe summary Pu-239 @ 9 - 10 ft

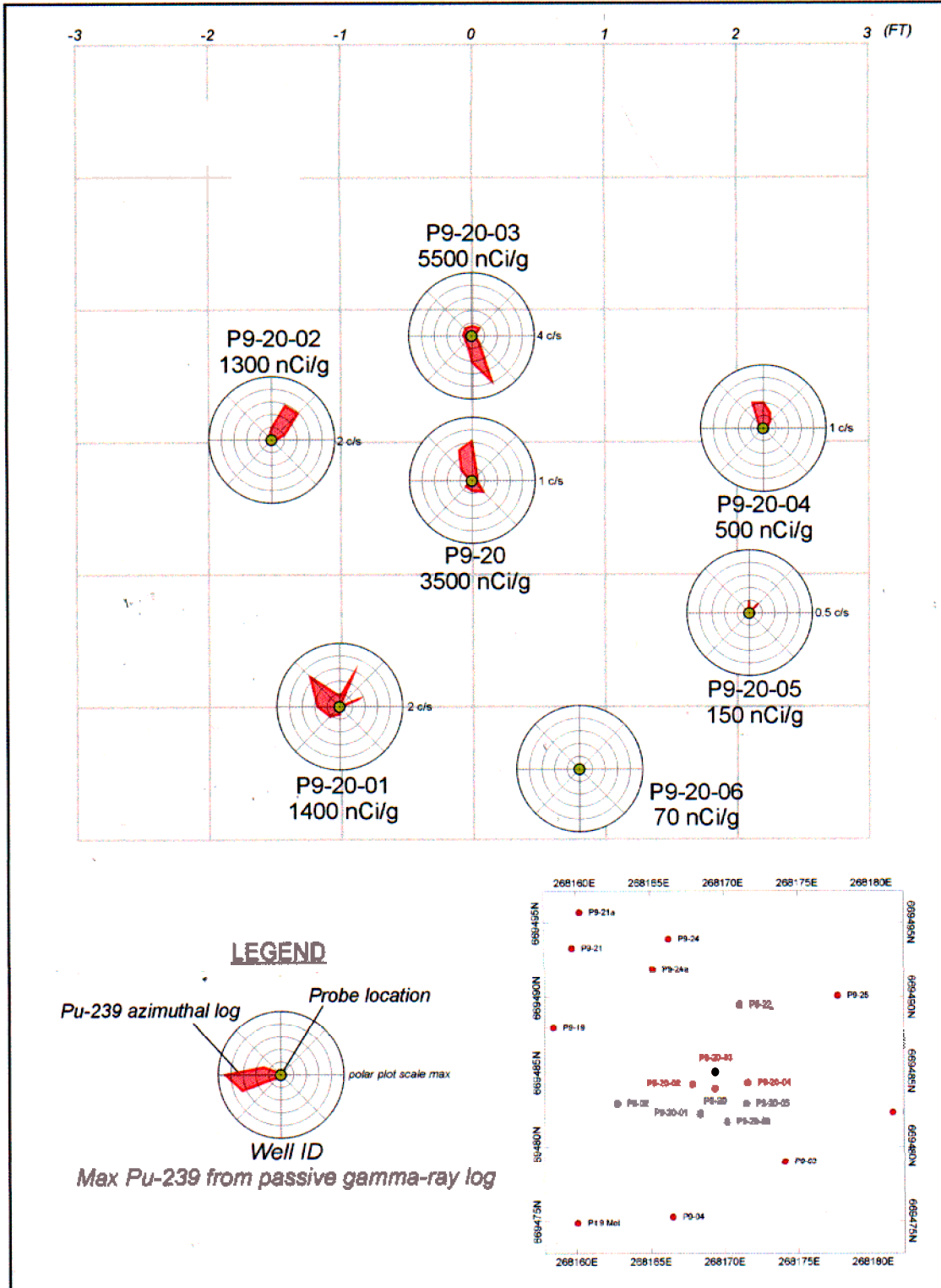


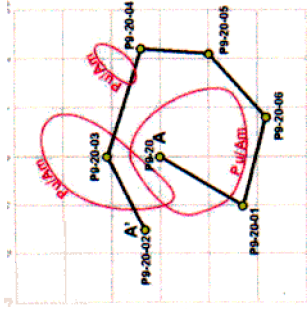
Figure 3-36. Azimuthal logging summary for the P9-20 probe cluster at 9-10 ft.

# P9-20 Cluster

## PROFILE A-A'

Pu/Am/Np, moisture and chlorine logs

6X horizontal exaggeration



**A**

**A'**

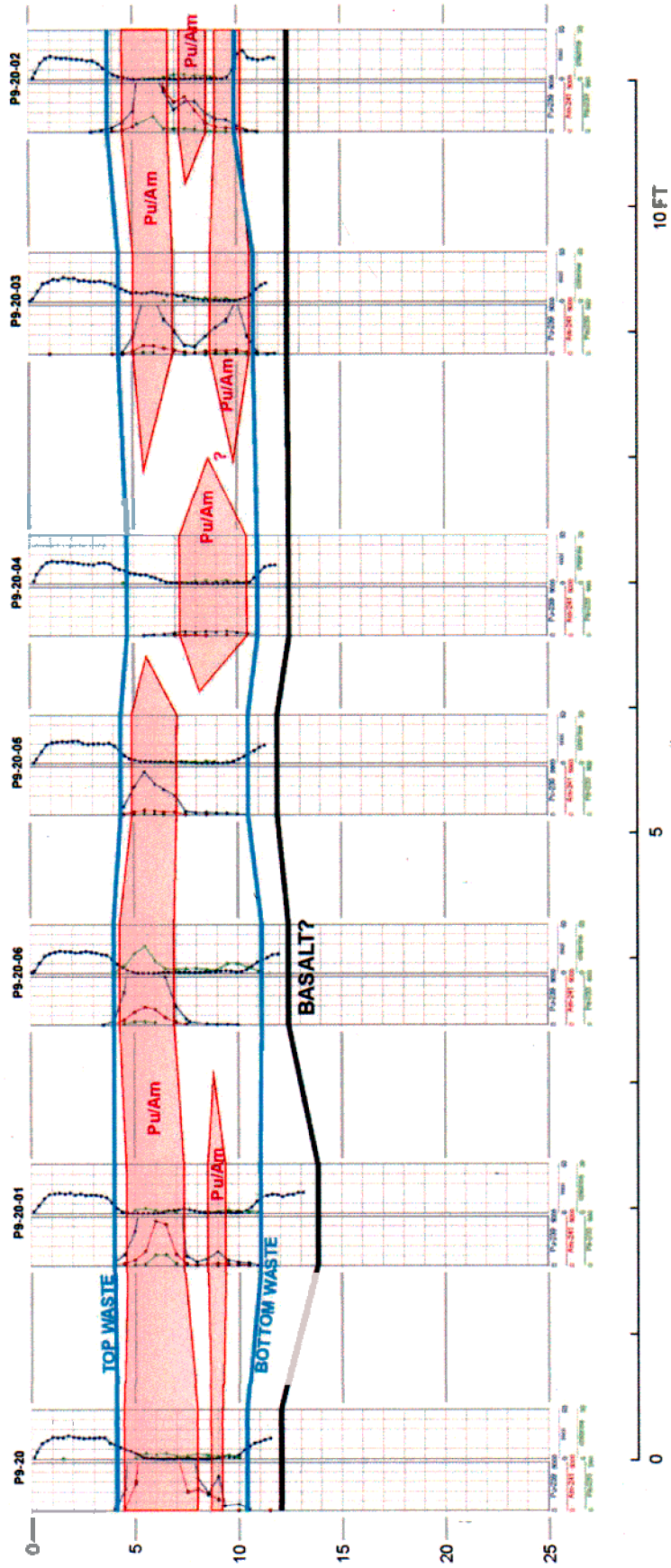


Figure 3-37. Spiral cross section through the P9-20 cluster probe.

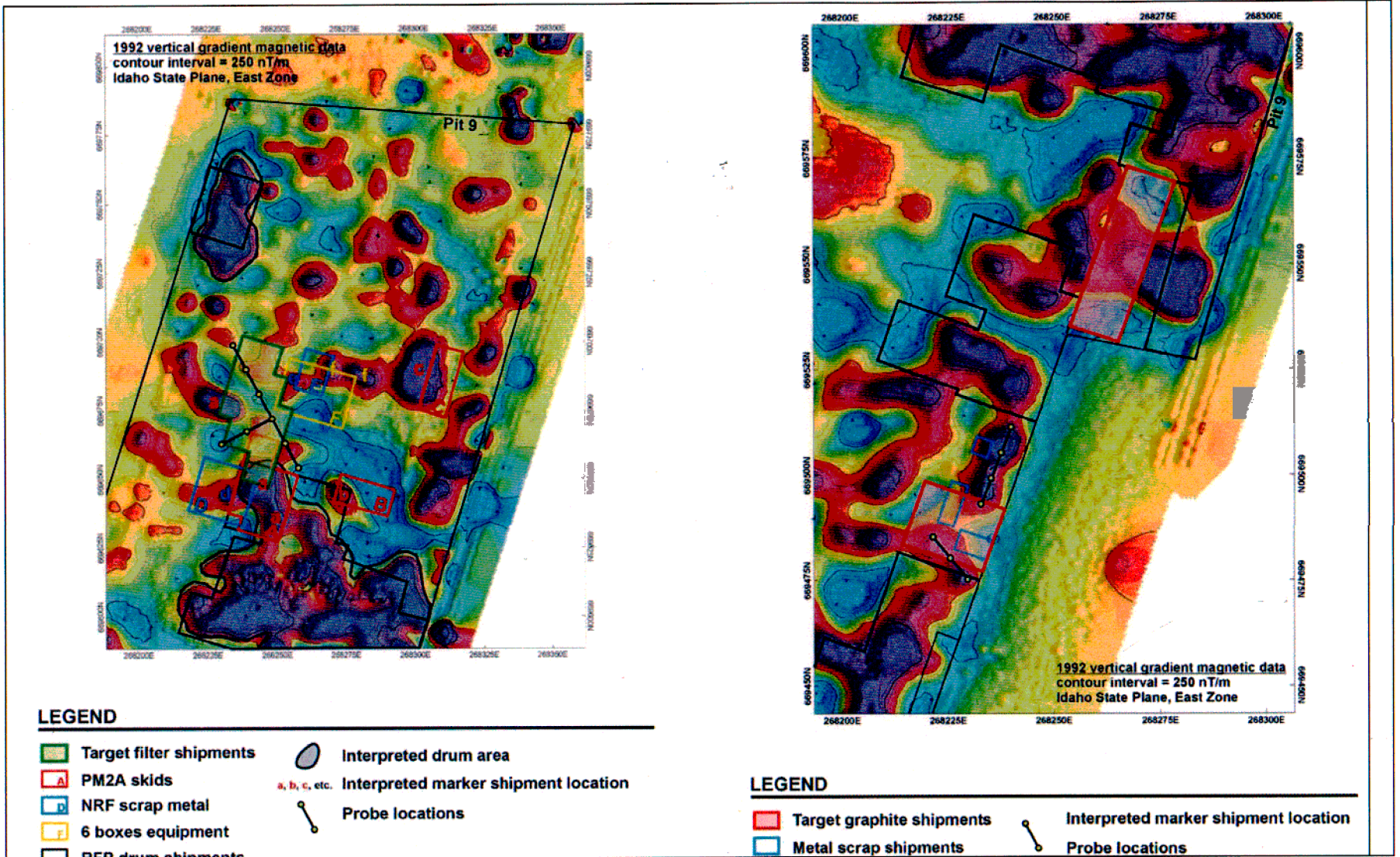


Figure 3-38. Surface geophysics for the Pit 9 Campaign 2 showing filter (left) and graphite (right) exploration areas. Final probe locations are also shown.

Two short probe transects were proposed to explore for the graphite drums. These transects utilize a total of seven probes with 8 ft between adjacent probes. The transects are positioned to intersect prominent geophysical anomalies in the immediate vicinity of the southern graphite shipment as defined by the inventory data. The southern graphite shipment was selected over the northern shipment because it contains a slightly higher percentage of graphite drums and because its position, as noted in the inventory record, appears to be more reliable than for the northern graphite shipment.

### 3.6.2 Observations on Radionuclide Contamination

The logging subcontractor conducted preliminary processing of the Pit 9 Campaign 2 logging data. Their processing included automated spectral analysis of passive gamma-ray data to identify the presence of specific target contaminants including  $^{235}\text{U}$ ,  $^{238}\text{U}$ ,  $^{239}\text{Pu}$ ,  $^{241}\text{Am}$ , and  $^{237}\text{Np}$ . After applying a standard calibration correction to convert net count rates to apparent radionuclide concentrations, summary results were compiled and delivered to the INEEL along with the raw spectral data.

Table 3-22 gives maximum detected levels of key target contaminants for all Pit 9 Campaign 2 probes. Blank cells indicate nondetects.

Table 3-22. Maximum apparent concentration values for Pit 9 Campaign 2 probes.

Well ID	Gross Count Rate	$^{235}\text{U}$ (pCi/g) <sup>a</sup>	$^{238}\text{U}$ (pCi/g) <sup>a</sup>	$^{239}\text{Pu}$ (nCi/g) <sup>a</sup>	$^{233}\text{Pa}$ (pCi/g) <sup>a</sup>	$^{241}\text{Am}$ (nCi/g) <sup>a</sup>	$^{137}\text{Cs}$ (pCi/g) <sup>a</sup>	$^{60}\text{Co}$ (pCi/g) <sup>a</sup>	CI_1165 (cps)
P9-FI-01	214	ND	ND	41.3	ND	ND	0.8	ND	2.4
P9-FI-02	1,749	ND	ND	1,678.0	2.5	171.8	ND	ND	4.0
P9-FI-03	5,731	ND	23.2	2,964.0	6.9	1,126.0	ND	ND	4.1
P9-FI-04	2,466	0.5	ND	2,155.0	6.9	359.2	3.0	ND	3.8
P9-FI-05	53,925	ND	ND	ND	ND	ND	1.6	814.2	0.5
P9-FI-06	17,392	ND	ND	ND	ND	ND	8.8	159.5	ND
P9-FI-07	12,844	ND	ND	11,994.0	34.4	1,388.0	ND	ND	3.7
P9-FI-08	211	ND	ND	ND	ND	ND	0.4	ND	ND
P9-GR-01	7,980	ND	33.2	1,252.0	126.6	5,111.0	ND	ND	ND
P9-GR-02	3,919	ND	49.3	714.6	68.1	2,273.0	ND	ND	ND
P9-GR-03	11,603	ND	ND	5,393.0	6.2	905.2	ND	ND	ND
P9-GR-04	266	ND	ND	ND	ND	ND	1.2	ND	0.9
P9-GR-05	460	ND	149.2	136.0	ND	111.5	ND	ND	18.2
P9-GR-06	1,087	ND	696.7	33.3	14.3	ND	2.5	4.8	6.0
P9-GR-07	1,192	ND	ND	1,046.0	7.2	132.6	ND	ND	0.4

a. Assumes homogenous, isotropic, and unconsolidated soil media.

ND = nondetect

The following observations are presented:

- Both  $^{235}\text{U}$  and  $^{238}\text{U}$  were detected in only a few probes at low levels.
- Pu, Am, and Np were detected in 11 of 15 probes; Pu levels in same range as for original P9 probes with high apparent concentration of 11,994 nCi/g measured in P9-FI-07. No Pu levels comparable to P9-20. Same general observations apply to Am. Np (as identified from  $^{233}\text{Pa}$ ) more widespread than in original P9 probes.
- Levels of  $^{137}\text{Cs}$  were detected in seven of 15 probes; maximum apparent concentration is 8.8 pCi/g in P9-FI-06.
- Levels of  $^{60}\text{Co}$  were detected in three of 15 probes, especially prominent in P9-FI-05 and P9-FI-06; this is the first appearance of significant  $^{60}\text{Co}$  levels anywhere in Pits 4, 9, and 10 logging data.
- Chlorine was detected in nine of 13 probes (two probes not yet logged with n-gamma tool); observed chlorine levels are consistent with original P9 probes.
- Am:Pu ratios were plotted for all Campaign 2 probes at all locations where both Am and Pu were detected above background (Figure 3-39). Graphite probes yield consistently higher Am:Pu ratios than filter probes, possibly reflecting a basic difference in waste type. Inventory records may contain information that can be used to ascertain if this Am:Pu ratio is diagnostic of either filter or graphite waste.
- P9-FI-02, P9-FI-03, P9-FI-04 and P9-FI-07, located near the center of the filter probe pattern, have the general radionuclide characteristics expected for contaminated filters (Figure 3-40). Probes P9-FI-01, P9-FI-05, P9-FI-06, and P9-FI-08, located at the ends of the probe pattern, have low or zero Pu, Am, and Np radionuclide levels and do not appear to be good candidates for filter waste. P9-FI-05 and P9-FI-06 may represent a distinctly different waste type based on the high  $^{60}\text{Co}$  levels.
- Figure 3-41 shows a cross section from P9-FI-01 through P9-FI-06. Note that increased Pu, Am, and Np levels correspond with decreases in Si, Ca, and K levels. Si, Ca, and K are common components of natural soil and can be used as indicators of the media characteristics surrounding the probe. Low media indicators show zones where soil is intermixed with or replaced by significant amounts of man-made waste material. Inventory records may help determine if the correspondence between high Pu, Am, and Np and low Si, Ca, and K is diagnostic for filter waste.
- Am:Pu ratios for graphite probes are compared with Am:Pu ratios for Probe P9-20, which is thought to represent characteristics of the graphite waste form (Figure 3-42). This plot shows that Probes P9-GR-03 and P9-GR-07 have similar Am:Pu ratios to P9-20. Figure 3-43 shows the location of these probes with respect to the targeted waste shipments and surface geophysics data.
- The media indicators, Si, Ca, and K, suggest that the contaminated zones in P9-GR-03 and P9-GR-07 have higher soil content than in P9-20 (Figure 3-43).

**3.6.2.1 Plutonium, Americium, and Neptunium** . Pu:Am and Am:Np apparent activity ratios for Pit 9 Campaign 2 probes are shown in Figure 3-44. Computed ratios assume homogenous conditions and do not account for differential attenuation of gamma rays.